

Axisymmetric flow between differentially rotating spheres in a dipole magnetic field

By N. KLEORIN¹, I. ROGACHEVSKII², A. RUZMAIKIN³,
A. M. SOWARD⁴ AND S. STARCHENKO⁵

¹Department of Mechanical Engineering, Ben-Gurion University of Negev, POB 653,
84105 Beer-Sheva, Israel

²The Racah Institute of Physics, The Hebrew University of Jerusalem, 91904, Jerusalem, Israel

³Jet Propulsion Laboratory, 4800, Oak Grove Drive, Pasadena, CA 91109, USA

⁴Department of Mathematics, University of Exeter, Laver Building, North Park Road,
Exeter EX4 4QE, UK

⁵Geophysical Observatory “Borok”, Yaroslavskaia obl. 152742, Russia

(Received 28 October 1996 and in revised form 8 April 1997)

Constant-density electrically conducting fluid is confined to a rapidly rotating spherical shell and is permeated by an axisymmetric potential magnetic field with dipole parity; the regions outside the shell are rigid insulators. Slow steady axisymmetric motion is driven by rotating the inner sphere at a slightly slower rate. Linear solutions of the governing magnetohydrodynamic equations are derived in the small Ekman number E -limit for values of the Elsasser number A less than order unity. Attention is restricted to the mainstream outside the Ekman–Hartmann layers adjacent to the inner and outer boundaries.

When $A \ll E^{1/2}$, MHD effects only lead to small perturbations of the well-known Proudman–Stewartson solution. Motion is geostrophic everywhere except in the $E^{1/3}$ shear layer containing the tangent cylinder to the inner sphere; that is embedded in thicker $E^{2/7}$ (interior), $E^{1/4}$ (exterior) viscous layers in which quasi-geostrophic adjustments are made. When $E^{1/2} \ll A \ll E^{1/3}$, those quasi-geostrophic layers become thinner $(E/A)^{1/2}$ Hartmann layers (inside only when $A > O(E^{3/7})$), across which the geostrophic shear is suppressed with increasing A ; they blend with the $E^{1/3}$ Stewartson layer at $A = O(E^{1/3})$. When $E^{1/3} \ll A \ll 1$, magnetogeostrophic adjustments are made in a thicker inviscid A -layer. Viscous effects are confined to the shrinking (blended) Hartmann–Stewartson layer; it consists of a column (stump) aligned to the tangent cylinder, attached to the equator, height $O((E/A^3)^{1/8})$ and width $O((E^3/A)^{1/8})$, supporting strong zonal winds.

With increasing A the main adjustment to the geostrophic flow occurs at $A = O(E^{1/2})$. When $E^{1/2} \ll A \ll 1$, the mainstream analogue to the non-magnetic Proudman solution is a state of rigid rotation, except for large quasi-geostrophic shears in (magnetic–Proudman) layers adjacent to but inside both the tangent cylinder and the equatorial ring of the outer sphere of widths $(E^{1/2}/A)^4$ and $(E^{1/2}/A)^{4/7}$ respectively; the former is swallowed up by the Hartmann layer when $A \geq O(E^{3/7})$.

1. Introduction

1.1. Historical perspective

The study of almost rigid rotation of a uniform incompressible viscous fluid confined between two concentric spheres rotating differentially about a common z^* -axis with angular velocities $(1 - \varepsilon)\Omega^*$ (inner) and Ω^* (outer) has a long history initiated by Proudman (1956). He argued that, in the rapid rotation limit of small Ekman number (2.1a)

$$E \ll 1, \quad (1.1)$$

viscous forces are negligible almost everywhere in the mainstream outside the thin $E^{1/2}$ -Ekman layers adjacent to the inner and outer boundaries. Their role is to translate the viscous boundary stress into an azimuthal momentum flux into (out of) the mainstream via Ekman pumping (sucking). The mainstream motion is almost everywhere geostrophic (i.e. azimuthal and independent of the axial coordinate z^*). We call the circular cylinders of radius s^* , on which the azimuthal geostrophic flow is constant everywhere, geostrophic cylinders. Geostrophic degeneracy is manifested by the unknown dependence of the fluid angular velocity $(1 - \varepsilon\Omega_G)\Omega^*$ on the radial coordinate s^* ; here Ω_G is the small dimensionless relative geostrophic rotation rate, which we refer to frequently below. Under steady-state conditions the degeneracy is resolved by balancing boundary friction at the top and bottom of each geostrophic cylinder ($\mathcal{S}_T = \mathcal{S}_B$ in (2.8) below – the Proudman balance). Consequently, fluid outside the tangent cylinder to the inner sphere (see figure 1 below) is stagnant, while inside the geostrophic angular velocity is intermediate between that of the inner and outer spheres, achieving the inner-sphere rotation rate at the tangent cylinder, across which motion suffers an abrupt discontinuity.

A striking feature of the Proudman solution is that the $O(E^{1/2})$ mainstream meridional motion inside the tangent cylinder induced by Ekman boundary layer pumping is itself geostrophic. Consequently, the associated streamlines are axial; they carry the fluid flux ejected from the bottom Ekman layer up to the top Ekman layer, where it is reabsorbed. As a result the bottom Ekman layer carries a net radial Ekman influx at the equator of the inner sphere; it acts as a sink for fluid, which has emerged from the corresponding source on the outer sphere. This source–sink combination leads to an axial jet on the tangent cylinder. The detailed nature of the resulting axial shear layers was resolved later by Stewartson (1966) (see also Philander 1971), following his earlier plane layer study of the ‘split-disc’ geometry (Stewartson 1957, but see also Greenspan 1968). Their main features are as follows. Thick quasi-geostrophic layers, controlled by the balance (see (3.4b) with $\lambda = 0$) of interior radial (s^*) friction (viscous effects) and top/bottom friction (i.e. the Ekman boundary conditions), remove the discontinuity in the azimuthal velocity and its radial derivative. The velocity jump is eliminated outside the tangent cylinder in an $E^{1/4}$ Stewartson layer, while the remaining shear discontinuity is removed inside the tangent cylinder, where the Ekman boundary layer on the inner sphere is singular, in a thinner $E^{2/7}$ Stewartson layer. Still, a discontinuity of the meridional fluid flux remains, which is removed in a thinner ageostrophic $E^{1/3}$ -layer. Finally we note that the equatorial Ekman layer singularity leads to that layer thickening to $O(E^{2/5})$ over an axial distance $O(E^{1/5})$ about the equator. These various layer length scales are illustrated in Stewartson (1966, figure 1).

When the fluid is electrically conducting and permeated by an applied axisymmetric meridional magnetic field, the resulting magnetohydrodynamic problem is characterized by an additional parameter, the Elsasser number Λ (2.1c) which provides a

measure of the magnetic field strength. The presence of the magnetic field modifies the character of the Ekman layer. The nature of the resulting Ekman–Hartmann layer was first investigated by Gilman & Benton (1968). Transient effects in a plane layer geometry were considered by Benton & Loper (1969), and Loper & Benton (1970). Steady Ekman layers on plane boundaries received further attention from Loper (1970*b*), while extensions to our spherical geometry were added by Loper (1970*a*); the main results, as they relate to our problem, are summarized in Appendix A.

Investigation of the MHD modifications to the axial shear layers was initiated by Vempaty & Loper (1975) in a rotating cylinder. In that study and a later investigation (Vempaty & Loper 1978) with Stewartson's (1957) split-disc geometry, the applied magnetic field is aligned to the rotation axis; MHD effects are only evident for large A . For a magnetic field with arbitrary orientation the magnetic field normal to the rotation vector is far more important, even when it is relatively weak. This is implied by the unpublished study by Kleeorin, Rogachevskii & Ruzmaikin referred to by Ruzmaikin (1993). To investigate this effect Hollerbach (1996) considered a plane layer of fluid permeated by a uniform magnetic field parallel to the boundaries, which are normal to the rotation. A rectangular analogue of Stewartson's (1957) split-disc geometry was considered. He applied spatially periodic velocity boundary conditions, which enabled him to resolve the axial shear layers using a Fourier series decomposition.

1.2. Summary of results

We restrict attention to the steady linear mainstream flow located outside the Ekman–Hartmann layers; all our detailed results are for the case $A \ll 1$ (3.1) for which they have an Ekman layer character. The essential idea is that, in this small- A limit, the bulk of the mainstream motion is geostrophic. The geostrophic degeneracy is resolved by considering the depth-averaged equation of motion (2.8) – the modified Taylor's (1963) condition (see §3.1). What remains is ageostrophic. Hollerbach (1996) identified three key parameter ranges: $A \ll E^{1/2}$, $E^{1/2} \ll A \ll E^{1/3}$ and $E^{1/3} \ll A \ll 1$. The scalings, which he isolated in these ranges, guide our investigation – though arguably Kleeorin, Rogachevskii & Ruzmaikin's earlier unpublished investigations provided him with some inspiration. We therefore call them the *weak*, *intermediate* and *strong field limits* respectively.

In the *weak field limit* $A \ll E^{1/2}$ (3.7) discussed in §3.2.1, the Lorentz force is sufficiently weak that the non-magnetic Proudman–Stewartson description continues to give the leading-order solution everywhere.

For $A = O(E^{1/2})$ discussed in §3.2.2, the Lorentz force becomes comparable in size with top/bottom friction. That magnetic–Proudman balance ($\mathcal{S}_T - \mathcal{S}_B = As^2 H \mathcal{L}[\Omega_G]$ in (2.8), (3.4)) resolves the geostrophic degeneracy throughout the bulk of the sphere. Elsewhere, only the $E^{1/4}$ Stewartson layer is significantly modified by the Lorentz force (see (3.14)).

For $E^{1/2} \ll A \ll 1$ discussed in §3.2.3, the Lorentz force dominates almost everywhere except in small axial shear layers. Consequently, Taylor's condition ($\mathcal{L}[\Omega_G] = 0$ in (3.4)) holds throughout the bulk of the fluid and is met trivially by a state of almost rigid rotation; essentially, the meridional magnetic field locks the fluid – a feature observed by Hollerbach (1994) and more recently by Dormy, Cardin & Jault (1997) in their numerical solutions. Its dimensionless relative angular velocity Ω^\dagger (3.16*b*) is determined by the condition that the torque on the inner and outer spheres be equal and opposite (see Appendices B and C). Departures from rigid rotation are

small, $\Omega_G - \Omega^\dagger = O(E^{1/2}/A)$, almost everywhere, consistent with Hollerbach's (1996) analytic results.

Throughout the *intermediate field limit* range $E^{1/2} \ll A \ll E^{1/3}$ several quasi-geostrophic adjustments are made, which we itemize separately.

For $E^{1/2} \ll A \ll E^{3/7}$ (3.18), large departures from rigid rotation are achieved in what we will call the E^2/A^4 magnetic–Proudman layer, where the geostrophic degeneracy is resolved by the magnetic–Proudman balance mentioned above. It is triggered inside the tangent cylinder by the equatorial Ekman layer singularity. As in the non-magnetic Proudman case, the geostrophic angular velocity adjusts across it to the inner-sphere angular velocity on the tangent cylinder (see (3.17)). The thinner radial friction layers take distinct forms (see (3.19) and figure 2*a*) on the two sides of the tangent cylinder; outside the tangent cylinder, an $(E/A)^{1/2}$ Hartmann layer accomplishes the angular velocity adjustment previously accommodated by the $E^{1/4}$ Stewartson layer, while inside the $E^{2/7}$ Stewartson layer continues with its non-magnetic role.

As A increases, the Hartmann length scale $O((E/A)^{1/2})$ shortens until at $A = O(E^{3/7})$ it has shrunk to $O(E^{2/7})$ – as has the $O(E^2/A^4)$ one. Accordingly, the magnetic–Proudman layer evaporates, being absorbed by the radial friction layers.

For $E^{3/7} \ll A \ll E^{1/3}$ (3.21), the geostrophic angular velocity no longer makes a significant excursion to meet the inner-sphere velocity on the tangent cylinder but instead remains close to the rigid rotation rate. Some small departures are accomplished in the remaining weak radial friction Hartmann layer (see (3.22) and figure 2*b*).

In the *intermediate field limit*, ageostrophic flow is confined to the $E^{1/3}$ Stewartson layer (see §4.2), which remains non-magnetic in character. Nevertheless, once A exceeds $O(E^{3/7})$ the failure of the geostrophic angular velocity to achieve the inner-sphere rotation rate on the tangent cylinder means that the Ekman flux that must be carried away from the equator increases by an order of magnitude, thereby considerably enhancing its strength and any features that it exhibits. In fact, inside and near the base of this $E^{1/3}$ Stewartson layer, large $O(\varepsilon\Omega^*)$ angular velocity adjustments are driven by magnetic and viscous forces; these ‘winds’ are terminated in the $E^{2/5}$ equatorial Ekman layer. The resulting intense ageostrophic angular velocity gradients in the winds focused close to the inner-sphere equator were overlooked by Hollerbach (1996).

At $A = O(E^{1/3})$, the Hartmann layer width shrinks to $O(E^{1/3})$ so becoming a Hartmann–Stewartson layer. With further increase of A its size decreases; it detaches itself from the outer sphere but remains as a stump on the tangent cylinder attached to the the equator of the inner sphere, where the shear discontinuity is its *raison d'être*.

In the *strong field limit* $E^{1/3} \ll A \ll 1$ (3.23), described largely in §4, a thinning $(E/A)^{1/2}$ Hartmann layer length scale may still be identified (see (4.7), (4.8)) but there does not appear to be any significant boundary layer structure linked to it (see §4.1). Nevertheless, two substantial ageostrophic layers clearly emerge. The larger is a thickening A -magnetogeostrophic layer (see §4.3), in which viscous forces play an insignificant role. It continues to thicken until it fills the shell, when $A = O(1)$ (see §4.5). The smaller is the (viscous) Hartmann–Stewartson layer stump, axial length $O(E^{1/8}/A^{3/8})$, radial width $O(E^{3/8}/A^{1/8})$ (see §4.4, (4.15) and figure 4), which detaches from the outer sphere and shrinks as A increases from $E^{1/3}$. The magnitudes of the shears that it supports (see (4.16*b*)) are comparable to the intense shears identified once A exceeds $E^{3/7}$, although they are limited to the axial extent of the stump.

Nevertheless, as z^* decreases, they intensify and reach their maximum independent of A at the base of the stump (see the case $|s - r_i| \rightarrow 0$ of (4.6b)), where the layer of intense shear contracts to its minimum on merging with the $E^{2/5}$ equatorial Ekman layer. In view of the other smoothing properties of the meridional magnetic field, this result comes as a surprise and may be of considerable significance (see §6) to the geodynamo application that we describe below.

Note in addition that throughout the range $E^{1/2} \ll A \ll 1$, there is a quasi-geostrophic $E^{2/7}/A^{4/7}$ magnetic–Proudman layer adjacent to the equator of the outer sphere, described in §3.3. Its role is to bring the almost constant geostrophic angular velocity up to speed with the outer sphere (see (3.28) and figure 3). Final minor adjustments are made, where the layer terminates, in an $E^{2/5}$ equatorial Ekman layer (see (3.30)).

We develop our spherical shell model for an applied axisymmetric potential magnetic field with dipole parity about the equatorial plane. It includes Hollerbach's (1994) special case of an axial dipole (2.7) employed in his numerical studies – also re-examined recently by Dormy *et al.* (1997). Since that dipole field drops off in intensity rapidly with radial distance, his results are sensitive to the inner to outer sphere radius ratio Δ ; for his case $\Delta := \frac{1}{3}$ (5.1c). Since the local Elsasser number drops by a factor Δ^6 (about 10^{-3} , see (5.1d)) between the inner and outer boundaries, it is difficult to attain clearly identifiable asymptotic regimes without adopting extremely small Ekman numbers. Indeed, even for the largest value of A used by Hollerbach (1994) the $E^{2/7}/A^{4/7}$ magnetic–Proudman layer adjacent to the equator of the outer sphere is not thin but occupies the entire region exterior to the tangent cylinder. Nevertheless, by reaching yet smaller Ekman numbers and larger Elsasser numbers Dormy *et al.* (1997) have achieved the required limit; their numerical results are excellent quantitative agreement with our asymptotics, as we explain in §5.

1.3. Geodynamo implications

An important motivation for the study is provided by the geodynamo. There fluid in the outer core is confined to a spherical shell while the rigid inner core is free to rotate relative to the solid mantle with possibly significant implications to core dynamics (Gubbins 1981; Steenbeck & Helmis 1975; Whaler & Holme 1996). The Earth's core system may lead to conditions similar to those of our problem, as Ruzmaikin (1989, 1993) and Nikitina & Ruzmaikin (1990) have pointed out. Indeed only recently has firm seismological evidence emerged that the inner core rotates faster than the mantle ($\varepsilon < 0$, see Song & Richards 1996; Su, Dziewonski & Jeanloz 1996).

Even before the differential rotation of the inner core and mantle was established it was recognized that the rigidity of the inner core plays an important role in the dynamo process. From their numerical results for mean-field axisymmetric dynamo calculations, Hollerbach & Jones (1993a) noted that, on the one hand, dynamo conditions can change their character across the tangent cylinder. On the other, Hollerbach & Jones (1993b, 1995) showed that the presence of an electrically conducting inner core can stabilize the dipole field against reversal. They also concluded that poloidal magnetic field reduces the strong shears across the tangent cylinder suggested by the Proudman–Stewartson results; asymptotic results valid at large magnetic Reynolds number, obtained by Starchenko (1993), support this conclusion. Anufriev (1994) developed these ideas further along lines proposed by Braginsky (1992), while Jault (1996) reports on possible inhibition of dynamo action caused by the presence of the inner solid core. From a general point of view, the asymptotics developed in this paper, like Hollerbach's (1996) before, argue that the poloidal magnetic field with moderate

Elsasser number will cause the tangent cylinder shear layers to largely evaporate. Nevertheless, there remains the strong stumpy Hartmann–Stewartson shear layer attached to the equator of the inner sphere, which we believe we are the first to identify; its existence is corroborated by Dormy *et al.*'s (1997) numerical results – their figure 6. The strong winds that they support may even provide some explanation for the intense shears found in Glatzmaier & Roberts' (1995*a,b*) fully three-dimensional numerical geodynamo calculations; we comment briefly on this matter in our concluding §6.

There are other implications, of course, for core–mantle coupling, for which topographic coupling, in particular, continues to be an exciting and controversial subject (Hide 1995*a,b*). The role of Ekman–Hartmann boundary layers in viscous and electromagnetic coupling has been discussed by Kleorin, Rogachevskii & Ruzmaikin (1993) amongst others. Nevertheless, in view of Song & Richards' (1996) results, it is essential also to understand inner (solid) and outer (fluid) core coupling; Glatzmaier & Roberts (1996*a,b*) have recently addressed this issue.

Finally, we note three important modifications to our model necessary for a more faithful representation of conditions in the Earth's core and comment briefly on the extent to which they affect our results.

First, the Earth's dynamo is generally believed to be of $\alpha\omega$ -type with the consequence that the azimuthal magnetic field is significantly larger than the meridional magnetic field by a factor of the large magnetic Reynolds number. Nevertheless, we have ignored it in our model. The reason is that, though the azimuthal magnetic field can drive magnetic winds, there is no direct feedback on the strong geostrophic flows that interest us, due to their alignment. This notion is supported by Vempaty & Loper's (1978) results for axial magnetic fields which also produce no coupling between geostrophic cylinders. It is our belief that the introduction of reasonable azimuthal magnetic field does not upset the key scalings that we predict.

Secondly, since the solid inner core is probably largely frozen iron, it is likely to have a conductivity comparable with that of the outer fluid core. As a consequence, the character of the Ekman–Hartmann layer on the inner core boundary assumed by us changes. For sufficiently large poloidal magnetic field the resulting strong electromagnetic coupling will lead to co-rotation of the inner and outer cores ($\Omega^\dagger \approx -1$) and so weaken the equatorial singularity on the inner sphere. Despite this striking modification of the magnetic Proudman solution, we anticipate that the other boundary layer structures that we predict continue to exist. Numerical results for this case have recently been reported by Dormy *et al.* (1997), which confirm the tendency towards co-rotation.

Thirdly, density variations must play an important role in the geophysical system. Indeed, the relative rotation rates of the inner and outer spheres is likely to be driven by thermal winds in the fluid core resulting from pole–equator temperature gradients (see Aurnou, Brito & Olson 1996). These appear to be set up in a natural way by asymmetric thermal convection; its distinct character inside and outside the tangent cylinder (see Olson & Glatzmaier 1995) is likely to aggravate the equatorial singularity as exemplified by the Glatzmaier & Roberts dynamo simulations (but see also Jones, Longbottom & Hollerbach 1995; Sarson, Jones & Longbottom 1997). On the other hand, we note that asymmetry in the magnetic field, such as an oblique dipole, or simply the addition of an axisymmetric quadrupole component, will lead to a radial component of magnetic field on the equator of the inner sphere, which will give the surface boundary layer a Hartmann character and so remove the equatorial singularity.

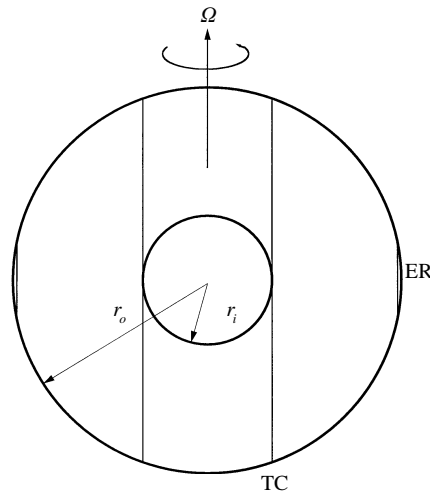


FIGURE 1. The shell geometry. The inner and outer spheres of radii r_i and r_o respectively are shown together with the location of the tangent cylinder TC and equatorial ring ER relative the rotation axis Ω .

2. Mathematical formulation of the problem

We consider the steady axisymmetric flow of constant-density ρ fluid with kinematic viscosity ν between two differentially rotating spheres. Relative to the frame rotating with angular velocity Ω^* , the outer sphere of radius L^*r_o is at rest, while the inner sphere of radius L^*r_i rotates with angular velocity $-\varepsilon\Omega^*$ ($\varepsilon \ll 1$); following Hollerbach (1996) L^* is the average of the sphere radii ($r_i + r_o := 2$) (see figure 1). The electrically conducting fluid with magnetic diffusivity η is permeated by an axisymmetric dipole field of typical magnitude B^* . The inner and outer boundaries are rigid insulators.

We adopt L^* , $L^*\Omega^*$ and B^* as our units of length, velocity $\varepsilon\mathbf{u}$ and magnetic field $\bar{\mathbf{b}} + \varepsilon E_\eta^{-1}\mathbf{b}$. Our system is characterized by the Ekman and Elsasser numbers

$$E := \frac{\nu}{L^{*2}\Omega^*}, \quad E_\eta := \frac{\eta}{L^{*2}\Omega^*} \quad \text{and} \quad A := \frac{\sigma B^{*2}}{\rho\Omega^*}, \quad (2.1a-c)$$

where $\sigma = 1/\mu\eta$ is the electrical conductivity. Motion is governed by the linear (with respect to ε) system of equations

$$2\hat{\mathbf{z}} \times \mathbf{u} = -\nabla p + A(\nabla \times \mathbf{b}) \times \bar{\mathbf{b}} + E\nabla^2\mathbf{u} \quad (\nabla \cdot \mathbf{u} = 0), \quad (2.2a)$$

$$0 = \nabla \times (\mathbf{u} \times \bar{\mathbf{b}}) + \nabla^2\mathbf{b} \quad (\nabla \cdot \mathbf{b} = 0), \quad (2.2b)$$

where the ‘hat’ is used to denote unit vector, p is the dimensionless pressure and we have used the fact that the applied magnetic field is potential, $\nabla \times \bar{\mathbf{b}} = 0$.

Relative to cylindrical polar coordinates (s, ϕ, z) , we set

$$\mathbf{u} := s\Omega\hat{\phi} + \nabla \times (s^{-1}\psi\hat{\phi}), \quad \mathbf{b} := sJ\hat{\phi} + \nabla \times (s^{-1}A\hat{\phi}), \quad \bar{\mathbf{b}} := \nabla \times (s^{-1}\bar{A}\hat{\phi}), \quad (2.3a-c)$$

where Ω , ψ , J , A and \bar{A} are functions of s and z alone. The corresponding toroidal

and poloidal decomposition of (2.2) is

$$-2\frac{\partial\psi}{\partial z} = -\frac{A}{s}\mathcal{J}(s^2J, \bar{A}) + E\mathcal{D}(s^2\Omega), \quad (2.4a)$$

$$2\frac{\partial\Omega}{\partial z} = \frac{A}{s}\mathcal{J}\left(\bar{A}, \frac{1}{s^2}\mathcal{D}A\right) + \frac{E}{s^2}\mathcal{D}^2\psi, \quad (2.4b)$$

$$0 = \mathcal{J}(\bar{A}, \Omega) + \frac{1}{s}\mathcal{D}(s^2J), \quad (2.4c)$$

$$\mathcal{J}(\psi, \bar{A}) = s\mathcal{D}A, \quad \mathbf{0} = \mathcal{D}\bar{A}, \quad (2.4d)$$

where \mathcal{J} and \mathcal{D} are the Jacobian and modified Laplacian operators defined by

$$\mathcal{J}(f, g) := \frac{\partial f}{\partial s}\frac{\partial g}{\partial z} - \frac{\partial f}{\partial z}\frac{\partial g}{\partial s} \equiv -(\nabla f \times \nabla g) \cdot \hat{\phi}, \quad (2.4e)$$

$$\mathcal{D}f := s\frac{\partial}{\partial s}\left(\frac{1}{s}\frac{\partial f}{\partial s}\right) + \frac{\partial^2 f}{\partial z^2} \equiv s\left(\nabla^2 - \frac{1}{s^2}\right)\frac{f}{s}. \quad (2.4f)$$

For some calculations we find it convenient to write the toroidal magnetic field in the form

$$sJ = s\Theta + \bar{b}_s\Phi, \quad (2.5a)$$

where Φ is related to the toroidal flow by

$$\Omega = -\frac{1}{s}\frac{\partial\Phi}{\partial s}; \quad (2.5b)$$

it is only uniquely determined up to an arbitrary function of z . From (2.4c), the new function Θ satisfies

$$\mathcal{D}(s^2\Theta) = 2\nabla\left(\frac{\partial\bar{A}}{\partial z}\right) \cdot \nabla\Phi + \nabla\bar{A} \cdot \nabla\left(\frac{\partial\Phi}{\partial z}\right). \quad (2.6)$$

The applied dipole magnetic field investigated by Hollerbach (1994) has radial- s and axial- z components

$$\bar{b}_s := -\frac{1}{s}\frac{\partial\bar{A}}{\partial z} = -r_i^3\frac{sz}{r^5}, \quad \bar{b}_z := \frac{1}{s}\frac{\partial\bar{A}}{\partial s} = -r_i^3\frac{2z^2 - s^2}{3r^5}, \quad (2.7a,b)$$

corresponding to the potential

$$\bar{A} := -r_i^3\frac{s^2}{3r^3}, \quad (2.7c)$$

where, relative to spherical polars (r, θ, ϕ) ,

$$s \equiv r \sin \theta, \quad z \equiv r \cos \theta. \quad (2.7d)$$

We restrict our discussions to the Northern hemisphere $0 < \theta < \frac{1}{2}\pi$. There, the ‘top’ boundary is $z_T := r_o \sin \theta$; the ‘bottom’ boundary is $z_B := r_i \sin \theta$ for $0 < s \leq r_i$ and $z_B := 0$ for $r_i \leq s < r_o$. Important in our subsequent analysis is the z -integral between the bottom and top boundaries of the ϕ -component (2.4a) of the momentum equation. It is the modified Taylor’s condition

$$\mathcal{S}_T - \mathcal{S}_B = \frac{1}{s}\frac{d}{ds} [s^2(\mathcal{M} + \mathcal{U})], \quad (2.8a)$$

where

$$\mathcal{M} := A \int_{z_B}^{z_T} s \bar{b}_s J \, dz, \quad \mathcal{U} := E \int_{z_B}^{z_T} s \frac{d\Omega}{ds} \, dz \quad (2.8b,c)$$

are the z -integrals of the ϕ -components of the Maxwell and viscous stresses on cylinders of radius s , while on the spherical surfaces

$$\mathcal{S} = - \left[2\psi + \frac{s^2}{\cos \theta} \left(A \bar{b}_r J + E \frac{\partial \Omega}{\partial r} \right) \right] \quad (2.8d)$$

is composed of the ϕ -components of momentum flux across the boundary, and Maxwell and viscous stresses on the boundary; \mathcal{S}_T and \mathcal{S}_B are its values on the top and bottom boundaries respectively. In our applications, the values of \mathcal{S} are evaluated outside the Ekman–Hartmann boundary layers and there the contribution made by the term proportional to $E \partial \Omega / \partial r$ is negligible.

At the inner and outer boundaries, the no-slip and insulating conditions yield the boundary conditions

$$\psi = \frac{\partial \psi}{\partial r} = J = 0 \quad \text{on } r = r_i \text{ and } r = r_o, \quad (2.9a)$$

$$\Omega = \begin{cases} -1 & \text{on } r = r_i; \\ 0 & \text{on } r = r_o. \end{cases} \quad (2.9b)$$

It is not necessary to specify the boundary conditions on A , because we only need the toroidal electric current $-s^{-1} \mathcal{D}A$ and do not need to solve for A itself. Note also, our symmetries are such that on the equatorial plane

$$\psi = \frac{\partial \Omega}{\partial z} = J = \mathcal{S}_B = 0 \quad \text{on } z = 0 \text{ for } r_i \leq s \leq r_o, \quad (2.9c)$$

while on the symmetry axis

$$\psi = 0, \quad \Omega \text{ and } J \text{ finite} \quad \text{on } s = 0 \text{ for } r_i \leq z \leq r_o. \quad (2.9d)$$

3. Quasi-geostrophic flow

In order to make analytic progress, we generally restrict attention to small Elsasser number

$$A \ll 1. \quad (3.1)$$

Then large gradients are confined to boundary layer regions, which include the Ekman–Hartmann boundary layers adjacent to the inner (i) and outer (o) spheres and vertical shear layers on the inner-sphere tangent cylinder $s = r_i$ and at the outer-sphere equator $s = r_o$.

The Ekman–Hartmann boundary layer solution, valid off the equators, is summarized in Appendix A. The jump conditions across the simplified Ekman layer, appropriate to the small Elsasser number limit (3.1), yield from (2.9) the reduced boundary conditions

$$\frac{\psi}{s^2} = \begin{cases} \text{finite} & \text{on } s = 0; \\ -\frac{E^{1/2}}{2(\cos \theta_o)^{1/2}} \Omega & \text{on } r = r_o; \\ \frac{E^{1/2}}{2(\cos \theta_i)^{1/2}} (\Omega + 1) & \text{on } r = r_i \quad (s < r_i); \\ 0 & \text{on } z = 0 \quad (s > r_i), \end{cases} \quad (3.2a)$$

$$J = O(E^{1/2}) \quad \text{everywhere on the boundary} \quad (3.2b)$$

on the mainstream solution valid outside the Ekman layer. The reduction in the number of boundary conditions is linked to the neglect of the z -derivatives in the viscous diffusion operator $E\mathcal{D}$ in (2.4a,b), but importantly they are retained in the magnetic diffusion operator in (2.4c,d). Note that (3.2a) is only uniformly valid down to the equator for magnetic fields with dipole symmetry, for which the radial magnetic field vanishes on the equator.

Within the framework of the reduced boundary conditions, motion in the bulk of the mainstream is geostrophic, becoming magnetogeostrophic when Λ increases to order unity. Throughout the range $\Lambda \leq O(1)$ the flow exhibits singularities on the tangent cylinder and the equatorial ring on the outer sphere (see figure 1). They are, in part, removed in quasi-geostrophic layers, which we discuss in this section. The yet smaller ageostrophic sublayers are investigated in §4.

3.1. Modified Taylor's condition

In our small E, Λ -limit, the Coriolis acceleration dominates and the terms on the right-hand side of (2.4b) are negligible. This is the Proudman–Taylor theorem and its consequence is that flow is geostrophic:

$$\Omega = \Omega_G(s) = -\frac{1}{s} \frac{d\Phi_G}{ds}, \quad \Phi = \Phi_G(s). \quad (3.3)$$

The magnetic induction equation (2.4c) with $\Omega = \Omega_G$, namely

$$\frac{1}{s^2} \mathcal{D}(s^2 J) = -\bar{b}_s \frac{d\Omega_G}{ds}, \quad (3.4a)$$

is solved for the azimuthal magnetic field sJ subject to the condition $sJ = 0$ everywhere on the boundary, namely (2.9) but importantly taken in the mainstream flow just outside the Ekman–Hartmann boundary layer. In this way, we determine the Maxwell stress \mathcal{M} as a functional \mathcal{L} of Ω_G . Accordingly from (2.8) Ω_G is the solution of the integro-differential equation

$$\frac{E}{Hs^3} \frac{d}{ds} \left(Hs^3 \frac{d\Omega_G}{ds} \right) + \Lambda \mathcal{L}[\Omega_G] = \frac{E^{1/2}}{H} [(\mathcal{B}_T + \mathcal{B}_B)\Omega_G + \mathcal{B}_B], \quad (3.4b)$$

where $\mathcal{B}_T \equiv \mathcal{B}_-$ and $\mathcal{B}_B \equiv \mathcal{B}_+$ are defined by (A3c) everywhere except on $z = 0$, $r_i < s < r_o$; there $\mathcal{B}_B = 0$ (see (2.9c)). The main obstacle to further progress is the determination of the functional

$$\mathcal{L}[\Omega_G] := \frac{1}{Hs^3} \frac{d}{ds} \int_{z_B}^{z_T} s^3 \bar{b}_s J \, dz, \quad (3.4c)$$

in which

$$H := z_T - z_B. \quad (3.4d)$$

Note, however, that there is one important global torque balance, which follows immediately from (3.4b) after multiplication by Hs^3 : upon integration over the entire hemispherical shell, the terms on the left-hand side vanish yielding the result

$$\int_0^{r_o} s^3 [(\mathcal{B}_T + \mathcal{B}_B)\Omega_G + \mathcal{B}_B] \, ds = 0. \quad (3.5)$$

This says that the total interior viscous and magnetic torques vanish; what remains is the balance of equal and opposite couples on the inner and outer spheres as determined from the Ekman–Hartmann jump conditions.

Unlike other mean-field studies involving modified Taylor conditions (see e.g. Jault 1995) for which there are additional source terms, in our case there appears to be no boundary layer on the axis $s = 0$. There, assuming the regularity of the solution in the form

$$\Omega_G(s) = \Omega_G(0) + O(s^2), \quad J(s, z) = J_0(z) + O(s^2), \quad (3.6a)$$

the balance (3.4b) yields the identity

$$\Omega_G(0) - \left(2HE^{1/2} \frac{d^2\Omega_G}{ds^2} \right)_{s=0} = -\frac{1}{2} - \frac{A}{E^{1/2}} \int_{r_i}^{r_o} \left(\frac{\partial \bar{b}_z}{\partial z} J \right)_{s=0} dz. \quad (3.6b)$$

In all our applications, we anticipate that the interior viscous term, here proportional to $E^{1/2}$, is negligible.

The main point to note is that the differential rotation $\Omega_G(s)$ is forced by the boundary condition through the right-hand side of (3.4b). Motion in the tangent cylinder, which is also governed by the modified Taylor's condition (3.4b), has important ramifications for the bulk of the quasi-geostrophic flow exterior to it; the outer equatorial ring has further implications.

3.2. The tangent cylinder

There are two limiting cases of small and large $A/E^{1/2}$, which we discuss below.

3.2.1. The weak field limit $A \ll E^{1/2}$

When

$$A \ll E^{1/2}, \quad (3.7)$$

the magnetic field simply perturbs the Proudman–Stewartson solution. For this, the internal torques in (3.4b) vanish everywhere; the remaining local torque balance on the inner and outer spheres yields the mainstream Proudman solution

$$\Omega_G(s) = \Omega_P(s) := -\frac{\mathcal{B}_B}{\mathcal{B}_B + \mathcal{B}_T}. \quad (3.8)$$

Its magnitude increases from $-\Omega_P = \frac{1}{2}$ on the symmetry axis $s = 0$ to $-\Omega_P = 1$ on the tangent cylinder $s = r_i$, while outside on $r_i < s < r_o$ it vanishes, $-\Omega_P = 0$. The discontinuous behaviour of the geostrophic flow on the tangent cylinder is determined from (A3c), namely

$$(\mathcal{B}_T + \mathcal{B}_B)\Omega_G + \mathcal{B}_B = \begin{cases} \left[\left(\frac{r_o}{H_i} \right)^{1/2} + \left(\frac{r_i}{2(r_i - s)} \right)^{1/4} \right] \Omega_G + \left(\frac{r_i}{2(r_i - s)} \right)^{1/4} & \text{for } s \uparrow r_i \\ \left(\frac{r_o}{H_i} \right)^{1/2} \Omega_G & \text{for } s \downarrow r_i, \end{cases} \quad (3.9a)$$

where

$$H_i := z_T(r_i) = (r_o^2 - r_i^2)^{1/2}. \quad (3.9b)$$

Here the interior viscous term is important above the inner sphere ($s < r_i$) in a layer of thickness $O(E^{2/7})$ and outside ($s > r_i$) in a layer of thickness $O(E^{1/4})$: the quasi-geostrophic Stewartson layers (see Stewartson 1966, figure 1).

With this Proudman–Stewartson flow we may calculate an $O(1)$ value of J from (3.4a) and the boundary condition $sJ = 0$. This in turn generates, via the modified

Taylor's condition (3.4b), a small $O(\Lambda/E^{1/2})$ correction to Ω_G consistent with the axial value given by (3.6b).

3.2.2. The magnetic–Proudman balance for $\Lambda = O(E^{1/2})$

As in the weak field limit, when

$$\Lambda = O(E^{1/2}), \quad (3.10)$$

the angular velocity Ω_G is of order unity. Likewise, the azimuthal magnetic field sJ induced by this motion is everywhere $O(1)$. Consequently, the term $\Lambda\mathcal{L}[\Omega_G]$ is comparable to the Ekman suction term on the right-hand side of (3.4b). This is the usual modified Taylor's condition balance as envisaged, for example, in the weakly nonlinear evolution of a mean-field dynamo relying on ω -quenching via the Malkus–Proctor (1975) mechanism.

It is instructive to discuss the nature of the tangent cylinder shear layers. Across them, the tangential z -component of electric field is continuous; specifically we note that

$$\frac{1}{s} \frac{\partial}{\partial s} (s^2 J) + \bar{b}_s \Omega_G \quad \text{is continuous across } s = r_i. \quad (3.11)$$

Accordingly, we may approximate the Lorentz force functional by

$$\Lambda\mathcal{L}[\Omega_G] = -A_i(\Omega_G - \Omega^\dagger), \quad (3.12a)$$

where

$$A_i := \frac{\Lambda}{H_i} \left(\int_0^{H_i} \bar{b}_s^2 dz \right)_{s=r_i} \quad (3.12b)$$

and Ω^\dagger is a constant, as yet unknown. From it, the magnetic extension of the Proudman solution at the tangent cylinder, valid outside the viscous shear layers, is the magnetogeostrophic solution

$$\Omega_G = \frac{A_i \Omega^\dagger - (E^{1/2}/H_i) \mathcal{B}_B}{A_i + (E^{1/2}/H_i) (\mathcal{B}_T + \mathcal{B}_B)} \quad \text{for } \delta_s \ll r_i - s \ll 1, \quad \delta_h \ll s - r_i \ll 1, \quad (3.13)$$

where δ_s is the $E^{2/7}$ Stewartson length (3.19b) below and δ_h is defined by (3.14b) below.

The Lorentz force term is negligible in the $E^{2/7}$ -layer above the inner sphere ($s < r_i$), where, as in the Stewartson solution, $\Omega_G \sim -1$, i.e. the rotation rate of the inner sphere. The details of the structure of this layer are explained in greater detail for their extension to the intermediate field limit (3.18) below. Outside ($s > r_i$), the hybrid $E^{1/4}$ Stewartson–Hartmann layer solution

$$1 + \Omega_G = \left(1 + \frac{A_i \delta_h^2}{E} \Omega^\dagger \right) \left[1 - \exp \left(- \frac{s - r_i}{\delta_h} \right) \right], \quad (3.14a)$$

where

$$\delta_h := E^{1/4} \left[\left(\frac{r_o}{H_i^3} \right)^{1/2} + \frac{A_i}{E^{1/2}} \right]^{-1/2}, \quad (3.14b)$$

indicates that Ω_G increases from -1 at $s = r_i$ to the value $(A_i \delta_h^2 / E) \Omega^\dagger$ of (3.13) as $(s - r_i) / \delta_h \uparrow \infty$. Determination of the value of Ω^\dagger requires knowledge of the solution

of the modified Taylor problem outside the quasi-geostrophic layers subject to the continuity condition (3.11). That is beyond the scope of the present analysis.

3.2.3. *The intermediate and strong field limit $E^{1/2} \ll A \ll 1$*

When

$$E^{1/2} \ll A \ll 1, \tag{3.15}$$

the dominant balance in (3.4b) is $\mathcal{L}[\Omega_G] = 0$, namely Taylor’s condition. It is satisfied trivially at lowest order by $\Omega_G = \Omega^\dagger = \text{constant}$, as suggested by (3.13) above. In fact, the mainstream solution has the form

$$\psi = E^{1/2} \tilde{\psi}, \quad \Omega = \Omega^\dagger + \frac{E^{1/2}}{A} \tilde{\Omega}_G(s), \quad J = \frac{E^{1/2}}{A} \tilde{J}. \tag{3.16a}$$

With $\Omega_G \sim \Omega^\dagger$ almost everywhere, we may determine its value from the global torque condition (3.5) as outlined in Appendix B. Setting $\mathcal{A} = 0$ in (B4) yields

$$\Omega^\dagger = -\frac{r_i^4}{r_i^4 + r_o^4}, \tag{3.16b}$$

in contrast to the weak field local result (3.8). As the tangent cylinder is approached, the order-one departures of Ω_G from Ω^\dagger predicted by (3.13) are given by

$$\frac{1 + \Omega_G}{1 + \Omega^\dagger} \sim \begin{cases} \left(\frac{r_i - s}{\delta_P}\right)^{1/4} / \left[1 + \left(\frac{r_i - s}{\delta_P}\right)^{1/4}\right] & \text{for } s < r_i \\ 1 & \text{for } s > r_i, \end{cases} \tag{3.17a}$$

in which

$$\delta_P := \frac{r_i}{2} \left(\frac{E^{1/2}}{H_i A_i}\right)^4 \quad (\equiv \delta_H^8 / \delta_S^7) \ll 1 \tag{3.17b}$$

(see (3.19b,c) below). On the short (by (3.15)) length δ_P the flow continues to exhibit Proudman’s singularity at the tangent cylinder ($s = r_i$) and so we call it the magnetic–Proudman layer; see figure 2(a).

Outside the tangent cylinder ($s > r_i$), the $E^{1/4}$ -layer thins with increasing A , taking on the character of a $(E/A)^{1/2}$ Hartmann layer, which continues to be represented by (3.14). In contrast, on the inside ($s < r_i$), the $E^{2/7}$ -layer continues to be non-magnetic as A is increased until $A = O(E^{3/7})$, at which value the magnetic–Proudman length $\delta_P = O(E^2/A^4)$ has shrunk to order $E^{2/7}$. In the range

$$E^{1/2} \ll A \ll E^{3/7}, \tag{3.18}$$

the solution exhibits similar characteristics to those found by Stewartson (1966); the new boundary layer structure is summarized in figure 2(a). Essentially, the geostrophic solution holds up to the edge of the $E^{2/7}$ -layer, where according to (3.13) the fluid co-rotates with the inner sphere ($\Omega_G \sim -1$). The main role of the thin interior $E^{2/7}$ -layer is to adjust the gradient of the shear velocity so that its gradient (in addition to its value) matches that of the thicker exterior $(E/A)^{1/2}$ -layer, in which the quasi-geostrophic velocity rapidly relaxes to $r_i \Omega^\dagger$. Stewartson’s (1966) inner solution,

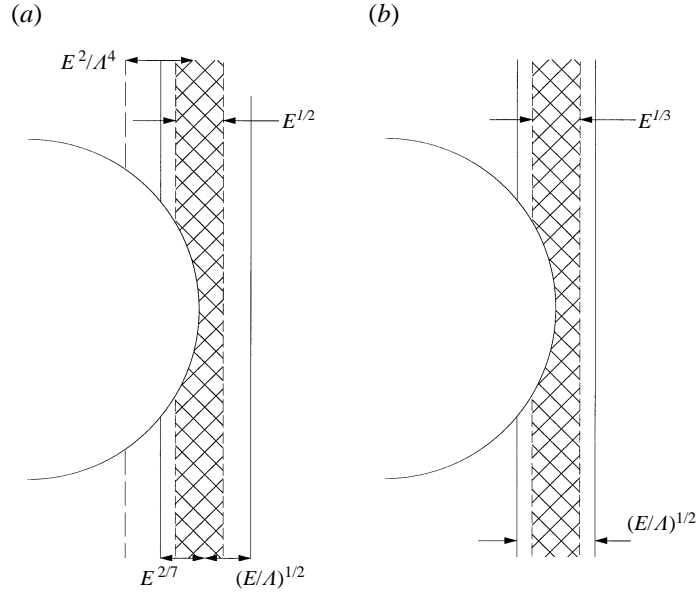


FIGURE 2. The tangent-cylinder boundary layer structure in the intermediate field limit. (a) $E^{1/2} \ll A \ll E^{3/7}$. The quasi-geostrophic interior $E^{2/7}$ Stewartson and exterior $(E/A)^{1/2}$ Hartmann layers are bounded by the solid lines. These layers abut the ageostrophic $E^{1/3}$ Stewartson layer, which is shown hatched. The E^2/A^4 magnetic–Proudman layer extends inwards as far as the broken lines. (b) $E^{3/7} \ll A \ll E^{1/3}$. As in (a), except that the interior Stewartson layer is now a Hartmann layer which has likewise absorbed the magnetogeostrophic layer.

modified with coefficients chosen to achieve matching with the outer solution (3.17), is

$$\frac{1 + \Omega_G}{1 + \Omega^{\dagger}} \sim \begin{cases} - \left(\frac{\delta_S}{\delta_H} \right) \frac{1}{\mathcal{F}'(0)} \mathcal{F} \left(\frac{r_i - s}{\delta_S} \right) + \left(\frac{\delta_S}{\delta_H} \right)^2 \mathcal{G} \left(\frac{r_i - s}{\delta_S} \right) & \text{for } s < r_i \\ 1 - \exp \left(- \frac{s - r_i}{\delta_H} \right) & \text{for } s > r_i, \end{cases} \quad (3.19a)$$

in which the Stewartson and Hartmann lengths

$$\delta_S := \left[(2/r_i)^{1/2} H_i^2 E \right]^{2/7}, \quad \delta_H := (E/A_i)^{1/2} \quad (3.19b,c)$$

satisfy

$$\delta_S \ll \delta_H \ll \delta_P \ll 1 \quad (3.19d)$$

and where \mathcal{F} and \mathcal{G} are the functions introduced by Stewartson (1966, equations (5.8) to (5.11)); the prime denotes derivative. Explicitly,

$$\mathcal{F}(\xi) := \frac{2 \left(\frac{4}{7} \right)^{4/7}}{\Gamma \left(\frac{4}{7} \right)} \xi^{1/2} K_{4/7} \left(\frac{8}{7} \xi^{7/8} \right) \quad (3.20a)$$

satisfies the homogeneous equation $\mathcal{F}'' - \xi^{-1/4} \mathcal{F} = 0$ with $\mathcal{F}(0) = 1$ and $\mathcal{F} \rightarrow 0$ as

$\xi \uparrow \infty$ with the consequence that $\mathcal{F}'(0) = -\left(\frac{4}{7}\right)^{1/7} \Gamma\left(\frac{3}{7}\right) / \Gamma\left(\frac{4}{7}\right)$, while

$$\mathcal{G}(\xi) := \frac{8}{7} \left\{ \xi^{1/2} \mathbf{K}_{4/7}\left(\frac{8}{7}\xi^{7/8}\right) \int_0^\xi \zeta^{1/2} \mathbf{I}_{4/7}\left(\frac{8}{7}\zeta^{7/8}\right) d\zeta + \xi^{1/2} \mathbf{I}_{4/7}\left(\frac{8}{7}\xi^{7/8}\right) \int_\xi^\infty \zeta^{1/2} \mathbf{K}_{4/7}\left(\frac{8}{7}\zeta^{7/8}\right) d\zeta \right\} \quad (3.20b)$$

satisfies the inhomogeneous equation $\mathcal{G}'' - \xi^{-1/4}\mathcal{G} = -1$ with $\mathcal{G}(0) = 0$ and $\mathcal{G} \sim \xi^{1/4}$ as $\xi \uparrow \infty$. Here $\mathbf{I}_{4/7}(\eta)$ and $\mathbf{K}_{4/7}(\eta)$ are Bessel functions of the first and second kind; we have used the Wronskian property $\eta(\mathbf{K}_{4/7}(\eta)\mathbf{I}'_{4/7}(\eta) - \mathbf{I}_{4/7}(\eta)\mathbf{K}'_{4/7}(\eta)) = 1$.

When $A = O(E^{3/7})$, all three boundary layer lengths δ_P , δ_H and δ_S are of comparable size, $O(E^{2/7})$, and abrupt changes in the geostrophic velocity in the vicinity of the tangent cylinder are reduced. For greater values, $E^{3/7} \ll A$, only the Hartmann layer remains (see figure 2*b*) and across it Ω_G remains close to Ω^\dagger . In the limited range

$$E^{3/7} \ll A \ll E^{1/3} \quad (3.21)$$

the resulting quasi-geostrophic Hartmann layer is sustained by the Ekman boundary condition on the inner sphere, forcing the weak response

$$\frac{\Omega_G - \Omega^\dagger}{1 + \Omega^\dagger} = -\frac{1}{2} \left(\frac{\delta_H}{\delta_S}\right)^{7/4} F\left(\frac{s - r_i}{\delta_H}\right) \quad \text{for } s - r_i = O(\delta_H), \quad (3.22a)$$

in which

$$\delta_P \ll \delta_H \ll \delta_S \ll 1 \quad (3.22b)$$

and where

$$F(\xi) := \begin{cases} \int_{-\infty}^0 |\xi'|^{-1/4} e^{-|\xi - \xi'|} d\xi' & \text{for } \xi \leq 0; \\ \Gamma\left(\frac{3}{4}\right) e^{-\xi} & \text{for } \xi \geq 0. \end{cases} \quad (3.22c)$$

In other words, inside the tangent cylinder ($s < r_i$) the singular behaviour (3.17) on the short magnetic–Proudman length δ_P has been swallowed up on the longer Hartmann layer length δ_H that replaces the even longer $E^{2/7}$ -scale δ_S across which viscous adjustments are made in the weaker field regime (3.18).

When

$$E^{1/3} \ll A \ll 1 \quad (3.23)$$

the strength of the Hartmann layer defined by (3.22*a*) evaporates. The remaining small adjustments are made in magnetogeostrophic and Hartmann–Stewartson layers illustrated in figure 4, whose nature we discuss in §4 below.

3.3. The equatorial ring

As the equator $s = r_o$ of the outer sphere is approached, the geostrophic angular velocity Ω_G must reduce to zero. In the intermediate and strong field limit (3.15) this happens across a magnetic–Proudman boundary layer of width

$$\delta_{Pe} := \frac{r_o}{2} \left(3 \frac{E^{1/2}}{r_o A_{eo}}\right)^{4/7} (\ll 1) \quad (3.24a)$$

illustrated on figure 3, where in the notation of (3.25*d*) below,

$$A_{eo} := Ar_o^2 \left(\frac{\partial \bar{b}_z}{\partial s}\right)_e^2. \quad (3.24b)$$

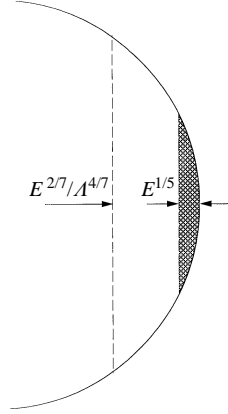


FIGURE 3. The equatorial ring in the intermediate and strong field limits $E^{1/2} \ll A \ll 1$. The outer edge of the $E^{2/7}/A^{4/7}$ magnetic–Proudman layer abuts the $E^{1/5}$ Stewartson layer shown hatched.

Assuming that the s -derivatives are large, the boundary layer approximation to (2.6) is simply $\partial^2 \Theta / \partial s^2 = 0$ with the trivial solution $\Theta = \Theta_0(z) + (r_o - s)\Theta_1(z)$. We assume that the mainstream solution is insensitive to the size of the small parameter $E^{1/2}/A$, so that matching with it yields an order-unity ratio Θ_1/Θ_0 independent of $E^{1/2}/A$. Consequently, on the short magnetic–Proudman length δ_{pe} (3.24), the second term proportional to $\Theta_1(z)$ is negligible. Upon composing the solution (2.5a) and applying the boundary condition $sJ = 0$ on $z \sim [2r_o(r_o - s)]^{1/2}$, we obtain

$$sJ \sim \left(\frac{\partial \bar{b}_z}{\partial s} \right)_e z \left[\varphi(\rho) - \varphi \left(\frac{z^2}{2r_o} \right) \right], \quad (3.25a)$$

where

$$\varphi(\rho) := \Phi(s), \quad \rho := r_o - s \quad (3.25b,c)$$

and we have assumed an applied potential field

$$\left(\frac{\partial \bar{b}_z}{\partial s} \right)_e := \left(\frac{\partial \bar{b}_z}{\partial s} \right)(r_o, 0) \equiv \left(\frac{\partial \bar{b}_s}{\partial z} \right)(r_o, 0) \quad (3.25d)$$

with dipole symmetry. From it, we may calculate the Maxwell stress (2.8b); after an integration by parts the following expression may be obtained:

$$\mathcal{M} = \frac{2A_{eo}}{3} \left(\frac{2}{r_o} \right)^{1/2} \int_0^\rho \rho^{3/2} \frac{d\varphi}{d\rho} d\rho. \quad (3.26)$$

From (3.4c) and (3.26) we obtain

$$A\mathcal{L}[\Omega_G] = -\frac{2A_{eo}}{3r_o} \rho(\Omega_G - \Omega^\dagger), \quad (3.27a)$$

where the constant of integration Ω^\dagger has been chosen as usual so that $\mathcal{L}[\Omega_G] \rightarrow 0$ as $\rho/\delta_{pe} \uparrow \infty$, where $\Omega_G \rightarrow \Omega^\dagger$. Accordingly, the modified Taylor's condition (3.4b) reduces to

$$\frac{E}{\rho^{1/2}} \frac{d}{d\rho} \left(\rho^{1/2} \frac{d\Omega_G}{d\rho} \right) - \frac{2A_{eo}}{3r_o} \rho(\Omega_G - \Omega^\dagger) = \frac{E^{1/2}}{2^{3/4} r_o^{1/4}} \frac{\Omega_G}{\rho^{3/4}}. \quad (3.27b)$$

The outer magnetic–Proudman solution corresponding to (3.17) is

$$\Omega_G = \frac{\Omega^\dagger}{1 + (\delta_{Pe}/\rho)^{7/4}} \quad \text{valid for } \rho = O(\delta_{Pe}). \quad (3.28)$$

As ρ decreases, it gives

$$\frac{\Omega_G}{\Omega^\dagger} \sim \left(\frac{\rho}{\delta_{Pe}}\right)^{7/4} \quad \text{for } \delta_{Se} \ll \rho \ll \delta_{Pe} \quad (3.29a)$$

valid until the interior viscous boundary layer is reached which is confined to the length

$$\delta_{Se} := \frac{r_o}{2} \left(\frac{4E^{1/2}}{r_o}\right)^{4/5} \quad (3.29b)$$

illustrated on figure 3. There the second radial derivative of Ω_G smooths out the remaining weak discontinuity in Stewartson’s $E^{2/5}$ -layer corresponding to the thickening Ekman layer. The motion is sustained by the Lorentz force with solution

$$\frac{\Omega_G}{\Omega^\dagger} = \left(\frac{\delta_{Se}}{\delta_{Pe}}\right)^{7/4} \mathcal{H}\left(\frac{\rho}{\delta_{Se}}\right), \quad (3.30a)$$

where

$$\mathcal{H}(\xi) := \frac{8}{5} \left\{ \xi^{1/4} \mathbf{K}_{2/5}\left(\frac{8}{5}\xi^{5/8}\right) \int_0^\xi \zeta^{7/4} \mathbf{I}_{2/5}\left(\frac{8}{5}\zeta^{5/8}\right) d\zeta + \xi^{1/4} \mathbf{I}_{2/5}\left(\frac{8}{5}\xi^{5/8}\right) \int_\xi^\infty \zeta^{7/4} \mathbf{K}_{2/5}\left(\frac{8}{5}\zeta^{5/8}\right) d\zeta \right\} \quad (3.30b)$$

satisfies the inhomogeneous equation $\xi^{-1/2}(\xi^{1/2} \mathcal{H}') - \xi^{-3/4} \mathcal{H} = -\xi$ with $\mathcal{H}(0) = 0$ and $\mathcal{H} \sim \xi^{7/4}$ as $\xi \uparrow \infty$; cf. our earlier result (3.20b).

Finally we note that the dominant balance in (2.4a) is

$$-2 \frac{\partial \psi}{\partial z} = Ar_o^2 \bar{b}_{ze} \frac{\partial J}{\partial z} \quad \text{with } \bar{b}_{ze} := \bar{b}_z(r_o, 0); \quad (3.31)$$

the terms proportional to $\partial J/\partial s$ are of lower order. Integration yields

$$\psi = -\frac{1}{2} Ar_o^2 \bar{b}_{ze} J. \quad (3.32)$$

This is the leading-order influence of the Lorentz force, from which we see that Taylor’s condition is satisfied trivially. The modified Taylor condition (3.27b) provides a higher-order balance of smaller terms.

4. Ageostrophic flow and Hartmann–Stewartson layers

In the absence of magnetic field the dominance of the geostrophic flow in the tangent-cylinder $E^{2/7}$ and $E^{1/4}$ Stewartson shear layers gives way to ageostrophic flow in thinner $E^{1/3}$ Stewartson layers. As the Elsasser number A is increased from zero, the magnetic field continues to induce only small perturbations of that ageostrophic flow until

$$A = O(E^{1/3}). \quad (4.1)$$

For this value all vertical shear layers blend with the same thickness and so we call the blend the Hartmann–Stewartson layer.

We outline briefly the equations governing the Hartmann–Stewartson layer. The

magnetic induction equation (2.4c) reduces as before to

$$\frac{\partial J}{\partial s} = -\bar{b}_s(\Omega - \Omega^\dagger). \quad (4.2)$$

In principle Ω^\dagger could be some function of z , but matching with the exterior geostrophic flow implies that it has the constant value (3.16b). Accordingly (2.4a,b) with (2.4c,d) yield

$$-2 \frac{\partial}{\partial z} \left(\frac{\psi}{r_i} \right) = \left(-A\bar{b}_s^2 + E \frac{\partial^2}{\partial s^2} \right) [r_i(\Omega - \Omega^\dagger)], \quad (4.3a)$$

$$2 \frac{\partial}{\partial z} [r_i(\Omega - \Omega^\dagger)] = \left(-A\bar{b}_s^2 + E \frac{\partial^2}{\partial s^2} \right) \left(\frac{1}{r_i} \frac{\partial^2 \psi}{\partial s^2} \right), \quad (4.3b)$$

while the Ekman boundary condition (3.2a) reduces to

$$\frac{\psi}{r_i} = \begin{cases} -\frac{E^{1/2}}{2} \left(\frac{r_o}{H_i} \right)^{1/2} r_i \Omega_{GT} & \text{on } z = H_i \\ \frac{E^{1/2}}{2} \left(\frac{r_i}{2(r_i - s)} \right)^{1/4} r_i (1 + \Omega_{GB}) & \text{on } z = [2r_i(r_i - s)]^{1/2} \text{ for } s < r_i \\ 0 & \text{on } z = 0 \text{ for } s > r_i, \end{cases} \quad (4.4)$$

where Ω_{GT} and Ω_{GB} are the values of the ageostrophic velocities on the tangent cylinder $s = r_i$ at the top and bottom boundaries respectively. It is important to remember that (4.2) and (4.3) are derived on the basis that $\partial/\partial s \gg \partial/\partial z$ appropriate to thin vertical layers. The terms on the right-hand side of (4.3b) are responsible for the zonal winds with singular behaviour at the equator.

Since $|r_i - s|$ is small, the bottom boundary condition implies that the value of ψ is an order of magnitude larger than $E^{1/2}$ in the shear layer. Consequently, we may approximate ψ to zero on the top boundary $z = H_i$. Also, within the framework of the same small value of $|r_i - s|$, we may apply the bottom boundary condition on $z = 0$. Thus following Stewartson (1966), we may obtain the solution of (4.3) by Fourier transform methods. It is

$$\frac{\psi}{r_i} = E^{1/2} \left(\frac{r_i}{2} \right)^{5/4} (1 + \Omega_{GB}) \int_{-\infty}^{\infty} \hat{\psi}_0(k) \frac{\sinh(k\hat{\chi}(k, z))}{\sinh(k\hat{\chi}_0(k))} e^{ik(s-r_i)} dk, \quad (4.5a)$$

$$r_i(\Omega - \Omega^\dagger) = -E^{1/2} \left(\frac{r_i}{2} \right)^{5/4} (1 + \Omega_{GB}) \int_{-\infty}^{\infty} k \hat{\psi}_0(k) \frac{\cosh(k\hat{\chi}(k, z))}{\sinh(k\hat{\chi}_0(k))} e^{ik(s-r_i)} dk, \quad (4.5b)$$

where

$$\hat{\psi}_0(k) := \frac{1}{\sqrt{2} \Gamma(\frac{1}{4}) (-ik)^{3/4}} \quad (4.5c)$$

is analytic in the upper half-plane with the complex plane cut along the negative imaginary axis ($(-ik)^{3/4} = e^{-i(3/8)\pi} k^{3/4}$ for positive real k) and

$$\hat{\chi}(k, z) := \frac{1}{2} \left(A \int_z^{H_i} \bar{b}_s^2(r_i, z) dz + Ek^2(H_i - z) \right), \quad (4.5d)$$

$$\hat{\chi}_0(k) := \hat{\chi}(k, 0) \equiv \frac{1}{2} (A_i + Ek^2) H_i \quad (4.5e)$$

(see (3.12b) above). For all our main applications with $A \gg E^{3/7}$, we have $\Omega_{GB} = \Omega^\dagger$. The reason for making a more general statement is to enable contact with weaker field results and, in particular, Stewartson's non-magnetic results, though application

to those cases requires some care. For example, in the non-magnetic case there is an additional linear shear, which is a trivial solution of (4.3) when $A = 0$ and is larger than that predicted by (4.5b). Then, of course, the Ω^\dagger term is irrelevant being absorbable in the linear shear (but see (4.10) and (4.11) below).

The most informative feature of this solution is the $z = 0$ value

$$r_i(\Omega - \Omega^\dagger)\Big|_{z=0} = -E^{1/2} \left(\frac{r_i}{2}\right)^{5/4} (1 + \Omega_{GB}) \int_{-\infty}^{\infty} k \widehat{\psi}_0(k) \coth(k \widehat{\chi}_0(k)) e^{ik(s-r_i)} dk \quad (4.6a)$$

of the azimuthal velocity. From it, we may deduce the asymptotic results

$$r_i(\Omega - \Omega^\dagger)\Big|_{z=0} \sim \begin{cases} -E^{1/2}(1 + \Omega_{GB}) \frac{r_i}{H_i A_i} \left(\frac{r_i}{2(r_i - s)}\right)^{1/4} & \text{as } s - r_i \downarrow -\infty \\ -E^{1/2}(1 + \Omega_{GB}) \frac{1}{4} \left(\frac{r_i}{2(r_i - s)}\right)^{5/4} & \text{as } s - r_i \uparrow 0 \\ E^{1/2}(1 + \Omega_{GB}) \frac{1}{2\sqrt{2}} \left(\frac{r_i}{2(s - r_i)}\right)^{5/4} & \text{as } s - r_i \downarrow 0 \\ 0 & \text{as } s - r_i \uparrow \infty. \end{cases} \quad (4.6b)$$

The large- $|s - r_i|$ asymptotic behaviour is geostrophic and predicted by (3.17) in the limit $|s - r_i| \gg \delta_P$, while the small- $|s - r_i|$ asymptotic behaviour is ageostrophic and was previously identified by Stewartson (1966, equation (6.23)) to occur within his $E^{1/3}$ -layers of the non-magnetic problem. Despite the strength of the small- $|s - r_i|$ singularity, he pointed out that it is compatible with the results for the thickening Ekman layer at the equator of the inner sphere.

The evaluation of the Fourier integrals (4.5a,b) and (4.6a) is achieved by distorting the integration contour in the complex plane. Contributions arise from integrating about the cut of $\widehat{\psi}_0(k)$ at the origin (traced to the boundary conditions) and the zeros of $\sinh(k \widehat{\chi}_0(k))$. The first zero

$$\widehat{\chi}_0(k) = 0, \quad \text{giving} \quad k = \pm i(E/A_i)^{1/2}, \quad (4.7a)$$

determines the Hartmann layer. The higher-order zeros

$$k \widehat{\chi}_0 \equiv \frac{1}{2}(A_i + Ek^2)kH_i = n\pi i \quad (n = 1, 2, \dots) \quad (4.7b)$$

determine the remaining boundary layer structures. The small- $|s - r_i|$ asymptotic result given in (4.6b) is slightly subtle and relies on approximating the integrand under the limit $|k| \rightarrow \infty$.

The formulae (4.5), (4.6) are powerful because of their generality. From them we may recover many of the results presented in §3 together with new ageostrophic flow and Hartmann–Stewartson layer results.

4.1. The role of the $(E/A)^{1/2}$ Hartmann layers

In the range $E^{1/2} \ll A \ll E^{3/7}$, (4.5) cannot be sensibly employed to resolve the Hartmann layer structure, since the geostrophic angular velocity Ω_{GB} is not constant to lowest order as the result (4.5) assumes. We must simply refer to our earlier result (3.19).

In the range $E^{3/7} \ll A \ll E^{1/3}$, we note that $k \widehat{\chi}(k, z)$ is $O((A_i^3/E)^{1/2})$ when $k = O((A/E)^{1/2})$ appropriate to the Hartmann layer length scale. With this small value, $\cosh(k \widehat{\chi}(k, z))$ in the integral (4.5b) is approximately unity independent of z . Using the Fourier convolution theorem we may recover our earlier quasi-geostrophic result (3.22).

In the strong field range $E^{1/3} \ll A \ll 1$, repeating the above argument, we may again express the result as a convolution integral but now the kernel is z -dependent. From a more general point of view, the roots of (4.7b) are now given approximately by

$$k \sim \begin{cases} \pm i(E/A_i)^{1/2} & \text{for integer } n = O(1). \\ i 2n\pi/(A_i H_i) \end{cases} \quad (4.8)$$

The former pair of roots again define the Hartmann layer, which is now very thin. Matching with the external flow yields the trivial linear z -independent solutions of vanishing strength as indicated by the intermediate field result (3.22). The latter single roots are responsible for the z -dependent structure of the thicker magnetogeostrophic layer discussed in §4.3 below. When, however, integer n is large, specifically

$$n = O((A_i/E^{1/3})^{3/8}), \quad (4.9)$$

the three roots are indistinguishable and they determine the structure of the Hartmann–Stewartson layer discussed in §4.4 below.

Essentially in the strong field range, the Hartmann layer plays a negligible role. The main adjustments are made in the thick magnetogeostrophic A -layer (see §4.3), while the remaining singular behaviour is removed in the small Hartmann–Stewartson layer (see §4.4).

4.2. $E^{1/3}$ Stewartson layers

Throughout the intermediate field regime $E^{1/2} \ll A \ll E^{1/3}$, we may determine the structure on the short $E^{1/3}$ Stewartson length scale illustrated in figures 2 and 3 by considering the contributions to the integrals (4.5) which occur when $k = O(E^{-1/3})$. Unlike the case for the thicker Hartmann layers, Ω_{GB} is constant across the layer and the objection raised in §4.1, about the use of (4.5) in the range $E^{1/2} \ll A \ll E^{3/7}$, is inapplicable. Under our $E^{1/3}k = O(1)$ approximation all terms proportional to A can be neglected. We, therefore, set

$$\widehat{\chi}(k, z) = \widehat{\chi}_E := \frac{1}{2}Ek^2(H_i - z) \quad (4.10a)$$

and essentially recover Stewartson's (1966, equation (6.22)) but with different constants of proportionality originating from the different bottom boundary condition. We may express the complete solution in the form

$$r_i(\Omega - \Omega_H) = -E^{1/2} \left(\frac{r_i}{2}\right)^{5/4} (1 + \Omega_{H0}) \int_{-\infty}^{\infty} k \widehat{\psi}_0(k) \frac{\cosh(k \widehat{\chi}_E(k, z))}{\sinh(k \widehat{\chi}_E(k, 0))} e^{ik(s-r_i)} dk, \quad (4.10b)$$

where

$$r_i \Omega_H = r_i \left(\Omega_{H0} + \Omega_{H1} \frac{s - r_i}{\delta_H} \right) \quad (\Omega_{GB} \equiv \Omega_{H0}) \quad (4.10c)$$

is the linear Hartmann layer contribution; δ_H is defined by (3.19c). The limiting forms of the coefficients are

$$\frac{1 + \Omega_{H0}}{1 + \Omega^\dagger} \sim \begin{cases} -(\delta_S/\delta_H) / \mathcal{F}'(0) & \text{for } E^{1/2} \ll A \ll E^{3/7} \\ 1 - \frac{1}{2}\Gamma(\frac{3}{4}) (\delta_H/\delta_S)^{7/4} & \text{for } E^{3/7} \ll A \ll E^{1/3} \end{cases} \quad (4.11a)$$

and

$$\frac{\Omega_{H1}}{1 + \Omega^\dagger} \sim \begin{cases} 1 & \text{for } E^{1/2} \ll A \ll E^{3/7} \\ \frac{1}{2}\Gamma(\frac{3}{4}) (\delta_H/\delta_S)^{7/4} & \text{for } E^{3/7} \ll A \ll E^{1/3}; \end{cases} \quad (4.11b)$$

δ_S is defined by (3.19b).

4.3. The magnetogeostrophic layer

In the strong field limit $E^{1/3} \ll A \ll 1$, a thicker A -magnetogeostrophic layer emerges; see figure 4. We may determine its (s, z) -structure by neglecting the term proportional to E in (4.5d), in the spirit of the third root taken in (4.8).

An alternative and illuminating procedure on this longer radial order- A length scale is to return to the full equations (4.3) and neglect the viscous terms. The remaining potential problem has the general solution

$$r_i(\Omega - \Omega^\dagger) + i \frac{1}{r_i} \frac{\partial \psi}{\partial s} = Z(\sigma), \tag{4.12a}$$

where Z is an analytic function of the complex variable

$$\sigma := s - r_i + i \frac{1}{2} A \int \bar{b}_s^2(r_i, z) dz = O(A). \tag{4.12b}$$

This representation is particularly useful in the neighbourhood of the equator of the inner sphere, where for applied potential magnetic fields with dipole symmetry σ has the asymptotic behaviour

$$\sigma = s - r_i + i \frac{A_{ei} z^3}{6r_i^2} \quad \text{with} \quad A_{ei} := Ar_i^2 \left(\frac{\partial \bar{b}_z}{\partial s} \right)^2 (r_i, 0). \tag{4.13}$$

The corresponding potential solution (4.12) satisfying (4.4) is

$$\frac{\psi}{r_i} = \frac{E^{1/2}}{2} r_i (1 + \Omega^\dagger) \left(\frac{r_i}{2|\sigma|} \right)^{1/4} \sqrt{2} \sin\left(\frac{1}{4}\vartheta\right), \tag{4.14a}$$

$$\Omega - \Omega^\dagger = \frac{E^{1/2}}{4} \frac{1 + \Omega^\dagger}{r_i} \left(\frac{r_i}{2|\sigma|} \right)^{5/4} \sqrt{2} \cos\left(\frac{5}{4}\vartheta\right), \tag{4.14b}$$

where

$$\sigma := |\sigma| e^{i\vartheta}. \tag{4.14c}$$

It recovers the power laws given by (4.6b) for $|s - r_i| \downarrow 0$. Note, however, that the alternative representation

$$\Omega - \Omega^\dagger = \frac{E^{1/2}}{2\sqrt{2}} \frac{1 + \Omega^\dagger}{r_i} \left(\frac{3r_i^3}{A_{ei} z^3} \right)^{5/4} \Upsilon(\vartheta), \tag{4.14d}$$

where

$$\Upsilon(\vartheta) := \sin^{5/4}\vartheta \cos\left(\frac{5}{4}\vartheta\right), \tag{4.14e}$$

usefully determines the angular velocity profile at fixed $z(> 0)$ with the radial distance given parametrically by

$$s - r_i = \frac{A_{ei} z^3}{6r_i^2} \cot \vartheta. \tag{4.14f}$$

As $s - r_i$ increases from $-\infty$ ($\vartheta = \pi$), the angular velocity Ω decreases ($\partial\Omega/\partial s < 0$) from Ω^\dagger attaining its minimum above the inner sphere ($Y = -0.72\dots$ at $\vartheta = 2\pi/3$); it increases ($\partial\Omega/\partial s > 0$) passing through Ω^\dagger outside the tangent cylinder (at $\vartheta = 2\pi/5$) attaining its maximum ($Y = 0.37\dots$ at $\vartheta = 2\pi/9$) and decreases again ($\partial\Omega/\partial s < 0$) to Ω^\dagger , as $s - r_i$ increases to ∞ ($\vartheta = 0$). The most striking feature of this result is the reversed flow $\Omega > \Omega^\dagger$ that it predicts sufficiently far outside the tangent cylinder.

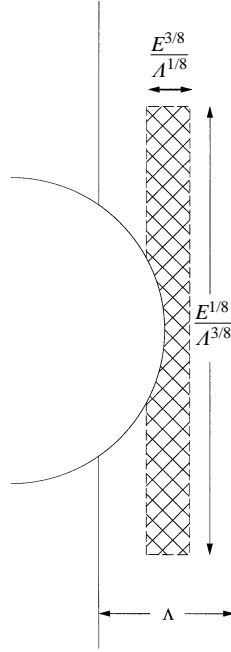


FIGURE 4. The tangent-cylinder boundary layer structure in the strong field limit $E^{1/3} \ll A \ll 1$. The A -magnetogeostrophic layer is bounded by the solid lines. The ‘stubby’ $E^{3/8}/A^{1/8}$ Hartmann–Stewartson layer stemming from the equator of size $O(E^{1/8}/A^{3/8})$ is shown hatched.

This reversed flow is confirmed by Dormy *et al.*’s (1997) numerical results – see their figure 6, but remember that the sign of their ε is opposite to ours.

4.4. The Hartmann–Stewartson layer

The solution (4.14) clearly illustrates the singular features of the magnetogeostrophic solution. The viscous terms are no longer negligible in a thin viscous sublayer attached to the equator of the inner sphere, where

$$s - r_i = O\left(\frac{E^{3/8}}{A_{ei}^{1/8}}\right), \quad z = O\left(\frac{E^{1/8}}{A_{ei}^{3/8}}\right); \quad (4.15)$$

see figure 4. Here the height $[2r_i(r_i - s)]^{1/2}$ of the inner-sphere surface remains small compared to the height of this viscous column and the result (4.5) continues to be applicable. Approximating the integrals on the basis that they are dominated by the contributions from large $k = O(A_{ei}^{1/8}/E^{3/8})$ yields

$$\frac{\psi}{r_i} = E^{1/2} \left(\frac{r_i}{2}\right)^{5/4} (1 + \Omega^\dagger) \int_{-\infty}^{\infty} \widehat{\psi}_0(k) e^{\Xi} dk, \quad (4.16a)$$

$$r_i(\Omega - \Omega^\dagger) = -E^{1/2} \left(\frac{r_i}{2}\right)^{5/4} (1 + \Omega^\dagger) \int_{-\infty}^{\infty} |k| \widehat{\psi}_0(k) e^{\Xi} dk, \quad (4.16b)$$

where

$$\Xi := ik(s - r_i) - \frac{1}{6} A_{ei} |k| (z^3/r_i^2) - \frac{1}{2} E |k|^3 z. \quad (4.16c)$$

In evaluating (4.16), we regard $|k|$ as an analytic function except for cuts along both imaginary axes excluding the origin $k = 0$ of the complex k -plane. Note that the

length scale estimates (4.15) anticipate that the dominant contribution to the integral occurs when each of the three terms defining \mathcal{E} is of order unity, cf. the arguments leading to the wavenumber estimate (4.9) for n .

Upon neglecting the viscous term proportional to E in (4.16c), we recover the magnetogeostrophic solution (4.14) valid outside the viscous sublayer. The point here is that as z decreases so does the radial component of the magnetic field. Hence locally the A -layer is thinning (width = $O(A_{ei}z^3)$) until it becomes comparable to that of the thickening Hartmann layer (width = $O(E^{1/2}/A_{ei}^{1/2}z)$). At that stage, the viscous Hartmann–Stewartson layer structure, first identified for the case $A = O(E^{1/3})$, re-emerges bounded on its outside by magnetogeostrophic flow. It should be stressed that even with the vanishing of \bar{b}_s the non-zero axial field \bar{b}_z plays an insignificant role. From another point of view, as A decreases, the size of the Hartmann–Stewartson layer increases until it extends to cover the entire tangent cylinder when $A = O(E^{1/3})$.

The integrals (4.16) are not easily evaluated except in special cases. They do, however, simplify on the tangent cylinder axis $s = r_i$. There, for small z , ignoring the magnetic term proportional to A_{ei} , we obtain

$$\frac{\psi}{r_i} \Big|_{s=r_i} = E^{5/12} \frac{\sqrt{2}\Gamma(\frac{1}{12}) \cos(3\pi/8)}{3\Gamma(\frac{1}{4})} \left(\frac{r_i}{2}\right)^{5/4} \left(\frac{2}{z}\right)^{1/12} (1 + \Omega^\dagger), \tag{4.17a}$$

$$r_i(\Omega - \Omega^\dagger) \Big|_{s=r_i} = -E^{1/12} \frac{\sqrt{2}\Gamma(\frac{5}{12}) \cos(3\pi/8)}{3\Gamma(\frac{1}{4})} \left(\frac{r_i}{2}\right)^{5/4} \left(\frac{2}{z}\right)^{5/12} (1 + \Omega^\dagger); \tag{4.17b}$$

these power laws – identified by Stewartson (1966, equation (6.29)) – are valid outside the equatorial Ekman layer $E^{1/5} \ll z \ll 1$.

Evidently, as Stewartson (1966) noted, viscosity does not remove the singularity in this ‘outer viscous’ sublayer, though it weakens it. More dramatically, the geostrophic flow velocity for $s \neq r_i$ is unmodified. So upon setting $z = 0$ in (4.16b) we again obtain the magnetogeostrophic result predicted by (4.14b) and given explicitly by ((4.6b)); the limits $s - r_i \uparrow 0$ and $\downarrow 0$).

The source of our difficulties may be traced to not applying the Ekman boundary condition correctly. We have simply perturbed about $\Omega = \Omega^\dagger$, which is clearly inadequate as the singularity is approached. This difficulty is finally resolved in the even smaller ‘inner viscous’ $E^{2/5}$ Stewartson layers on the equator, not illustrated in our figures – but see Stewartson’s (1966 figure 1).

4.5. Elsasser number order unity

We conclude with some comments about the interesting limit

$$A = O(1). \tag{4.18}$$

Everywhere, outside the Ekman–Hartmann layers and their Hartmann–Stewartson equatorial extensions on the inner and outer boundaries, the solution takes the form

$$\psi := E^{1/2}\tilde{\psi}(s, z), \quad \Omega := \Omega^\dagger + E^{1/2}\tilde{\Omega}(s, z), \quad A := E^{1/2}\tilde{A}(s, z), \quad J := E^{1/2}\tilde{J}(s, z), \tag{4.19}$$

where the new tilded variables satisfy (2.4) with the viscous terms proportional to E ignored. They are to be solved subject to the Ekman–Hartmann boundary layer jump

A	0.25	1.0	4.0	16.0
$\frac{4}{9}A^6A$	0.0002	0.0006	0.0024	0.0098
$\frac{4}{9}A$	0.1111	0.4444	1.7778	7.1111
A_i	0.015	0.06	0.25	0.98

TABLE 1. Boundary layer characteristics for Hollerbach’s (1994) Elsasser numbers.

condition (A3a), which in the complex notation of Appendix A is

$$\left(-\frac{\tilde{J}}{b_r} + i\frac{\tilde{\psi}}{s^2} \right) \Big|_{r=r_w} = \pm \frac{\Omega_w - \Omega^\dagger}{\lambda_w}. \tag{4.20}$$

Though the size of two equatorial Hartmann–Stewartson layers shrinks to zero as $E \downarrow 0$, they leave awkward singularities. At the equator to the outer sphere, $\tilde{\psi}$ remains non-zero. Its value is reduced to zero across the $E^{2/7}$ magnetic–Proudman layer identified in §3.3 with solution (3.28). At the equator of the inner sphere, both $\tilde{\psi}$ and particularly $\tilde{\Omega}$ exhibit singularities as described above in §§4.3, 4.4. Despite the singularities, the reduced mathematical problem appears to be well posed though its numerical solution may be hard to implement. To that end the introduction of $E^{1/2}\tilde{\Phi}$ in (2.5b) might remove some of the singularity exhibited by Ω . Certainly, it could help for the strong field case $E^{1/3} \ll A \ll 1$, for which $\tilde{\Omega} = \tilde{\Omega}_G(s)$ outside the magnetogeostrophic layer. There $\tilde{\Omega}_G$ is singular, whereas $\tilde{\Phi}$ is finite and continuous across the layer.

5. Hollerbach’s numerical model

We largely limit our comparisons to Hollerbach’s (1994) numerical results portrayed in his figure 4, for the case

$$E := 10^{-4}, \tag{5.1a}$$

with

$$r_i := \frac{1}{2} \quad \text{and} \quad r_o := \frac{3}{2} \tag{5.1b}$$

giving the radius ratio

$$A := \frac{r_i}{r_o} = \frac{1}{3}. \tag{5.1c}$$

His product AR_m is our A ; its values in his four sets of figures are listed in our table 1. In applying the Ekman–Hartmann jump conditions at the outer and inner boundaries, the parameters which measure the importance of magnetic effects are $\frac{4}{9}A^6A \cos \theta$ and $\frac{4}{9}A \cos \theta$ respectively; see table 1, where significantly

$$A^6 = 3^{-6} = 0.0013717\dots \tag{5.1d}$$

So in all cases the outer wall layer is an Ekman layer. In contrast, the inner wall layer exhibits magnetic effects and is clearly in the Ekman–Hartmann regime for the final two cases.

To determine the appropriate shear layer regime, we need the ratio

$$\frac{A_i}{A} = \int_0^{\cos^{-1}(1/3)} \sin^2\theta \cos^6\theta \, d\theta = \frac{5\pi}{2^8} - \frac{1}{7 \cdot 3^7} + \dots = 0.0613\dots \tag{5.2}$$

The values of A_i – see table 1 – are all arguably large compared to $E^{1/2} = 0.01$ and small compared to unity as required by our asymptotics. Since we also have $E^{3/7} = 0.02$, $E^{1/3} = 0.046$, we may speculate that the smallest table 1 value $A_i = 0.015$ corresponds to the intermediate field regime, in which a substantial shear discontinuity should still persist; the table 1 value $A_i = 0.06$ corresponds to the transition regime between intermediate and strong fields; while the largest table 1 values $A_i = 0.25$ and 0.98 should correspond to the strong field regimes for which the magnetogeostrophic region is expanding to fill the sphere.

If the mainstream flow is in almost rigid rotation with angular velocity Ω^\dagger , the torque balance on the inner and outer spheres gives

$$\Omega^\dagger \approx -0.012 \tag{5.3}$$

for weak magnetic fields; see (3.16*b*) – (B6*a*). In Hollerbach’s (1994) strongest field case $A = 16.0$, the generalized result – (B6*b*) – may be more appropriate. It is based on the assumption that the outer boundary supports an Ekman layer, while in contrast the inner boundary supports a Hartmann layer. The notion is supported by the corresponding inner-sphere torque estimate $\mathcal{T}_+ \sim \frac{2}{3}\pi r_i^4 (EA)^{1/2} (1 + \Omega^\dagger) \approx 0.0052(1 + \Omega^\dagger)$ (see (B2*b*) and (B3*b*)); it yields Hollerbach’s (1994, table 2) value 0.004831 when $\Omega^\dagger \approx -0.077$. Since Hollerbach claims that his motion is almost rigid body rotation, this result is compatible with the fact that the one distinguishable contour $\Omega = -1/15 \approx -0.067$ of the last of his figures 4 lies outside the tangent cylinder. Despite this agreement the corresponding estimate $\Omega^\dagger \sim -(7/16)\Delta^4 A^{1/2} \approx -0.022$ though of slightly larger magnitude than (5.3) still remains small compared to Hollerbach’s rough estimate of $1/15$. A similar discrepancy is apparent in Dormy *et al.*’s (1997) largest A -case illustrated in their figure 6.

A clue to the explanation of the discrepancy can be seen the contour plot for ψ in Hollerbach’s figures 4. On the outer sphere – but outside the boundary layer – where $\psi = \psi_o$, its maximum occurs close to the tangent cylinder. For the almost pure Ekman layer on the outer sphere, the result (A3) indicates that, while Ω remains constant, the analytic value ψ_o continues to increase. Only when the outer equatorial ring layers are reached does ψ_o decrease; it does so in concert with the magnitude $|\Omega_G|$ of the geostrophic angular velocity, which is brought into co-rotation with the outer sphere. Since, however, the magnetic field is relatively weak near the outer sphere, the magnetic–Proudman layer there is very thick; according to (3.24) and (2.7*b*), its width is

$$\frac{\delta_{Pe}}{r_o} = \frac{1}{2} \left(\frac{2E^{1/2}}{\Delta^6 A} \right)^{4/7}, \tag{5.4}$$

giving $\delta_{Pe} \approx 0.7112$ for the strongest field case $A = 16.0$. It indicates that departures from almost rigid rotation occur at radial distance $r_o - \delta_{Pe} \approx 0.7888$, which is tantalizingly close to the inner-sphere radius $r_i = 0.5$ compatible with Hollerbach’s ψ -plots. For each of the weaker field cases the magnetic–Proudman length δ_{Pe} increases by factor $2^{8/7}$. It means that even though Hollerbach indicates that a substantial part of the flow – in his strongest field case – is close to rigid rotation, it must make significant adjustments in the outer regions, as indicated by our §3.3 results. Since the torque integral on the outer sphere is heavily weighted in that region, it is reduced by a very large factor which can easily (and must!) account for the discrepancy noted. In Appendix C, we attempt to quantify the corrections due to the existence of the outer magnetic–Proudman layer. Though the tendency to increase Ω^\dagger is clearly predicted by (C3), the expansion parameter $2\delta_{Pe}/r_o$ is never small in any

E^{DCJ}	A^{DCJ}			δ_{se}/r_o
	0.1	1.0	10.0	
10^{-3}	0.3052	0.0819	0.0220	0.0956
10^{-4}	0.1581	0.0424	0.0114	0.0381
10^{-5}	0.0819	0.0220	0.0059	0.0152
10^{-6}	0.0424	–	–	0.0060

TABLE 2. δ_{pe}/r_o for various values of E^{DCJ} and A^{DCJ} . The values of the $E^{2/5}$ Stewartson length δ_{se}/r_o are included for comparison.

of Hollerbach's cases as required by the asymptotics. Consequently, no quantitative comparison is justified. Nevertheless, the result does emphasize the sensitivity of the torque balance to this outer region. We stress these points because Hollerbach draws attention to the closeness of his numerical solution to a state of rigid rotation.

The central issue is the small size of $A = \frac{1}{3}$; Hollerbach (1994) has not reached the asymptotic regime assumed in our development. Though we can make useful comparisons of some features, it is important to appreciate the limitations. The most significant is that isolated above, namely that outside the tangent cylinder he has not attained the thin magnetic–Proudman equatorial ring layer limit $\delta_{pe} \ll 1$ necessary for the validity of the §3.3 asymptotic analysis. Dormy *et al.* (1997), on the other hand, clearly obtain this asymptotic limit. To make comparisons we note that their Ekman and Elsasser numbers are related to ours by

$$E^{\text{DCJ}} = E/r_o^2 \quad \text{and} \quad A^{\text{DCJ}} = A^6 A/r_o^2 \quad (5.5)$$

respectively. The corresponding values of δ_{pe}/r_o for the values of A^{DCJ} used in Dormy *et al.*'s (1997) figures 13 and 16 – but larger than those (5.3a) employed by Hollerbach (1994) – are listed in table 2, where $E = 2.25E^{\text{DCJ}}$, $A^6 A = 2.25A^{\text{DCJ}}$ ($A = 1640.25A^{\text{DCJ}}$).

Significantly, (3.28) implies that δ_{pe}/r_o is the distance in their units from the outer sphere at which the rotation rate is one half the value outside the magnetic–Proudman layer. On that basis the comparison is remarkably sharp. Furthermore, their figure 12 confirms that the zonal flow in this layer is geostrophic for the case $E^{\text{DCJ}} = 10^{-5}$. Note, however, that the $E^{2/5}$ Stewartson layer is of relatively wide thickness δ_{se}/r_o (see (3.29b)) and only lies convincingly inside the magnetic–Proudman layer for the weakest field case $A^{\text{DCJ}} = 0.1$. For the other cases, $A^{\text{DCJ}} = 1.0$ and 10.0, interior radial friction clearly smooths out the solution. It also explains why the $(r_o - s)^{7/4}$ behaviour predicted by (3.29a) is not discernible as $s \uparrow r_o$. Despite the viscous smoothing the numerical results provide convincing vindication of our magnetic–Proudman layer solution.

6. Geophysical implications

Whereas the magnitude of the differential rotation is never greater than the relative velocities of the inner and outer spheres, its gradient may achieve larger values. Across the tangent cylinder the peak value order-of-magnitude estimates

$$O(\Omega - \Omega^\dagger) = \begin{cases} 1 & \text{when } A \leq O(E^{3/7}) \\ A^{-7/8} E^{3/8} & \text{for } E^{3/7} \leq A \leq E^{1/3} \\ E^{1/12} & \text{when } A = O(E^{1/3}) \\ A^{5/32} E^{1/32} & \text{for } E^{1/3} \leq A \leq 1 \end{cases} \quad (6.1a)$$

and

$$O\left(\frac{\partial\Omega}{\partial s}\right) = \begin{cases} E^{-1/4} & \text{when } A \leq O(E^{1/2}) \\ A^{1/2}E^{-1/2} & \text{for } E^{1/2} \ll A \ll E^{3/7} \\ E^{-2/7} & \text{when } A = O(E^{3/7}) \\ A^{-3/8}E^{-1/8} & \text{for } E^{3/7} \ll A \ll E^{1/3} \\ E^{-1/4} & \text{when } A = O(E^{1/3}) \\ A^{9/32}E^{-11/32} & \text{for } E^{1/3} \ll A \ll 1 \end{cases} \quad (6.1b)$$

can be identified as follows. In the *weak field* regime ($A \ll E^{1/2}$) the largest gradients occur in the $E^{-1/4}$ Stewartson layer and magnitudes are fixed by (3.14). In the *intermediate field* regime they occur in the Hartmann layer; the magnitudes are fixed by (3.19) in the range ($E^{1/2} \ll A \ll E^{3/7}$) and (3.22) in the range ($E^{3/7} \ll A \ll E^{1/3}$). The results show that the large shear is associated with the geostrophic velocity $\Omega_G(s)$ and is suppressed by the magnetic field in Hartmann layers. In the *strong field* regime ($E^{1/3} \ll A \ll 1$), the strong shears are limited to the Hartmann–Stewartson layer stump attached to the equator of the inner core. We estimate sizes of $\Omega(s, z)$ and $\partial\Omega/\partial s$ on the basis of the inner core boundary results given by the limit $|s - r_i| \downarrow 0$ of (4.6b) evaluated on the stump width $O(E^{3/8}/A^{1/8})$ (see (4.15)). In this small stump, the shear remains strong though localized by the strengthening of the magnetic field; this result contrasts dramatically with the suppression caused by the Hartmann layers in the *intermediate field* regime.

There is one important qualification to the above estimates, which are based on typical values in the various regions. For all values of A , the strongest shears are located on the tangent cylinder at the edge of the $E^{2/5}$ equatorial Ekman layer. There at $z = O(E^{1/5})$ (4.6b) gives $\Omega - \Omega^\dagger = O(1 + \Omega_{GB})$ and $\partial\Omega/\partial s = O((1 + \Omega_{GB})E^{-2/5})$. This equatorial singularity is relatively weak for $A \ll E^{3/7}$, since Ω_{GB} is close to -1 . When $A \gg E^{3/7}$, however, Ω_{GB} is close to Ω^\dagger . Thus the shear gradient near the equator $z = 0$ is of order $E^{-2/5}$ independent of A ; it decreases rapidly with increasing z along the tangent cylinder. Indeed, when $A \gg E^{1/3}$ that rate of decrease is enhanced as reflected by the decrease in length of the Hartmann–Stewartson layer stump. The essential point is that though the meridional magnetic field acts to reduce the shear throughout the bulk of the fluid shell, it exacerbates the angular velocity jump across the inner-sphere Ekman–Hartmann layer so strengthening the equatorial singularity. This idea is confirmed by Dormy *et al.*'s (1997) numerical investigations, where the second of their figures 6 illustrates the strong shear and even the overshooting behaviour that we predicted from (4.14).

The intensification of the shear for $A \gg E^{3/7}$ leads to strong inductive effects, which may even lead to ‘runaway’ growth of the dynamo. By that we mean that magnetic field generation leads to a positive feedback. This concept has long been recognized in the case of convective dynamos (Eltayeb & Roberts 1970), and has often been used to argue that the Elsasser number A be at least of order unity for dynamo equilibration (see e.g. Roberts 1988). Nevertheless, the idea must be applied in our context cautiously, as the cross-sectional area $O(E^{1/2}/A^{1/2})$ of the Hartmann–Stewartson layer stump (see (4.15)) decreases with increasing A above $E^{1/3}$; therefore, the total inductive effect appears to decrease. Nevertheless, we have clearly identified a mechanism for intensifying shear in the neighbourhood of the equator to the inner sphere, which may explain features of recent numerical results (Glatzmaier & Roberts 1995a,b, 1996a,b). We end, however, with a cautionary remark. Those calculations (also Sarson *et al.* 1997) involve the use of hyperdiffusivity on toroidal surfaces. This means that, on the one hand, Ekman–Hartmann layers are faithfully reproduced;

on the other, radial friction is significantly enhanced with the consequence that the axial shear layers discussed in this paper are thickened considerably. Essentially, for comparison purposes a larger effective Ekman number is required in the formula (6.1).

Andrew Soward acknowledges the support of the SERC grant number GR/K06495. Sergey Starchenko is grateful to the University of Newcastle upon Tyne for the award of a Research Fellowship, 15 January 1995 to 14 January 1996; he also acknowledges the support of the Russian Fund of Fundamental Research (RFFI). We have benefited from discussions with Dave Loper concerning his pioneering contributions to the subject and with Rainer Hollerbach about his important developments. We wish to thank Emmanuel Dormy, Philippe Cardin and Dominique Jault for providing us with a preprint of their paper. We have also benefited from related discussions with Sasha Anufriev, Gary Glatzmaier, Dominique Jault, Chris Jones and Paul Roberts. We thank Yuri Shteimler for valuable discussions of asymptotic methods, though Keith Stewartson's (1966) seminal paper provided the blueprint for our asymptotic solution.

Appendix A. The Ekman–Hartmann layers

We summarize the results for the Ekman–Hartmann layers adjacent to the inner and outer spheres appropriate to our analysis. Assuming the dominance of the radial derivatives, (2.4c) integrates giving $\partial J/\partial r = -\bar{b}_r(\Omega - \Omega_{\pm})$, where the subscript \pm indicates mainstream values just outside the boundary layers on the inner (+) and outer (−) spheres. In this way (2.4a,b) reduce to

$$-\frac{2 \cos \theta}{s^2} \frac{\partial \psi}{\partial r} = -A \bar{b}_r^2 (\Omega - \Omega_{\pm}) + E \frac{\partial^2 \Omega}{\partial r^2}, \quad (\text{A } 1a)$$

$$2s^2 \cos \theta (\Omega - \Omega_{\pm}) = -A \bar{b}_r^2 \frac{\partial \psi}{\partial r} + E \frac{\partial^3 \psi}{\partial r^3}, \quad (\text{A } 1b)$$

In the conventional complex notation, the solution satisfying the mainstream and wall (w) boundary conditions is

$$(\Omega - \Omega_{\pm}) + \frac{i}{s^2} \frac{\partial \psi}{\partial r} = (\Omega_w - \Omega_{\pm}) \exp [\mp \lambda_w (r - r_w)/E^{1/2}], \quad (\text{A } 2a)$$

where

$$\lambda_w^2 := A \bar{b}_r^2 + 2i \cos \theta \quad (\text{Re } \lambda_w > 0). \quad (\text{A } 2b)$$

For Hollerbach's (1994) dipole field (2.7), it is

$$\lambda_w^2 = \cos \theta \left(2i + \frac{4}{9} A [r_i/r_w]^6 \cos \theta \right) \quad \left(\bar{b}_r = -\frac{2}{3} [r_i/r_w]^3 \cos \theta \right). \quad (\text{A } 2c)$$

Integration across the boundary layer applying the boundary conditions $\psi = J = 0$ on $r = r_w$ ($w = i$ or o) yields the important results

$$\left(-\frac{J}{\bar{b}_r} + i \frac{\psi}{s^2} \right)_{r=r_w} = \pm E^{1/2} \frac{\Omega_w - \Omega_{\pm}}{\lambda_w}, \quad (\text{A } 3a)$$

$$\mathcal{S}_{\pm} = \pm E^{1/2} s^2 \mathcal{B}_{\pm} (\Omega_{\pm} - \Omega_{\pm}), \quad (\text{A } 3b)$$

where

$$\cos \theta \mathcal{B}_{\pm} := \operatorname{Re} \lambda_w = \begin{cases} (\cos \theta)^{1/2} + O(\Delta) & \text{for } \Delta \ll 1; \\ \frac{2}{3} \Delta^{1/2} (r_i/r_w)^3 \cos \theta + O(\Delta^{-1/2}) & \text{for } \Delta \gg 1 \end{cases} \quad (\text{A } 3c)$$

for their mainstream values at the edges of the Ekman–Hartmann boundary layers.

Appendix B. Torque balance: almost rigid rotation

When

$$\Delta \gg E^{1/2}, \quad (\text{B } 1)$$

the mainstream flow is in almost rigid rotation Ω^\dagger . Within the framework of that approximation the dimensionless torques \mathcal{T}_+ (on the inner sphere) and \mathcal{T}_- (on the outer sphere) reduce via (A3) to

$$\mathcal{T}_{\pm} := \mp 4\pi \int_0^{r_w} s \mathcal{S}_{\pm} ds = 4\pi E^{1/2} (\Omega^\dagger - \Omega_w) \int_0^{r_w} s^3 \mathcal{B}_{\pm} ds \quad (\text{B } 2a)$$

yielding

$$\mathcal{T}_{\pm} = 4\pi E^{1/2} r_w^4 (\Omega^\dagger - \Omega_w) \mathcal{V} \left(\frac{2}{3} \Delta^{1/2} (r_i/r_w)^3 \right), \quad (\text{B } 2b)$$

where \mathcal{V} is a function of a single variable:

$$\mathcal{V}(x) := \operatorname{Re} \left\{ \int_0^{\pi/2} (x^2 \cos^2 \theta + 2i \cos \theta)^{1/2} \sin^3 \theta d\theta \right\}. \quad (\text{B } 3a)$$

Its asymptotic forms are

$$\mathcal{V}(x) = \begin{cases} \frac{8}{21} & \text{for the Ekman limit } x \ll 1 \\ \frac{1}{4} x & \text{for the Hartmann limit } x \gg 1. \end{cases} \quad (\text{B } 3b)$$

Since the torques on the spheres are equal in magnitude but opposite in sign. The global torque balance (3.5), equivalently $\mathcal{T}_+ = -\mathcal{T}_-$, implies that

$$\Omega^\dagger = - \left[1 + \frac{\mathcal{V} \left(\frac{2}{3} \Delta^{1/2} \Delta^3 \right)}{\Delta^4 \mathcal{V} \left(\frac{2}{3} \Delta^{1/2} \right)} \right]^{-1} \left(\Delta := \frac{r_i}{r_o} \right). \quad (\text{B } 4)$$

For small Δ ,

$$\Delta \ll 1, \quad (\text{B } 5)$$

we may distinguish three limiting cases:

$$\Omega^\dagger \sim \begin{cases} -\Delta^4 & \text{for the Ekman limit } \Delta \ll 1 & (\text{B } 6a) \\ -\frac{7}{16} \Delta^4 \Delta^{1/2} & \text{for } 1 \ll \Delta \ll \Delta^{-6} & (\text{B } 6b) \\ -\Delta & \text{for the Hartmann limit } \Delta^{-6} \ll \Delta; & (\text{B } 6c) \end{cases}$$

the middle case is hybrid – the inner and outer boundaries have Hartmann and Ekman characters respectively.

Appendix C. Torque balance modification due to the magnetic–Proudman layer

In the large-gap limit

$$E^{1/2}r_o^{-1} \ll \Delta^6 A \ll 1 \quad (\text{C } 1)$$

the outer magnetic–Proudman layer width δ_{Pe} (3.24) remains small compared to the outer-sphere radius r_o for Hollerbach’s (1994) dipole field (2.7), while the outer-sphere boundary layer has an Ekman layer character. The torque on the outer sphere, which takes into account the outer magnetic–Proudman layer solution (3.28), is

$$\mathcal{T}_- = 4\pi E^{1/2}r_o^4 \Omega^\dagger \left[\mathcal{V}(0) - \int_0^{\pi/2} \frac{\delta_{Pe}^{7/4}}{\rho^{7/4} + \delta_{Pe}^{7/4}} (\cos \theta)^{1/2} \sin^3 \theta \, d\theta \right], \quad (\text{C } 2a)$$

in the notation of §3.3 and Appendix B. Asymptotic evaluation on the basis that $\delta_{Pe} \ll r_o$ yields with (B3a) the result

$$\mathcal{T}_- = \frac{32\pi}{21} E^{1/2} r_o^4 \Omega^\dagger \left[1 - \left(\frac{3\pi}{4 \sin(3\pi/7)} \right) \left(\frac{2\delta_{Pe}}{r_o} \right)^{3/4} \right]. \quad (\text{C } 2b)$$

In our limit (C1), (B6b) is modified to

$$\Omega^\dagger = -\frac{7}{16} \Delta^4 A^{1/2} \left[1 + \left(\frac{3\pi}{4 \sin(3\pi/7)} \right) \left(\frac{2\delta_{Pe}}{r_o} \right)^{3/4} \right] \quad \text{with} \quad \delta_{Pe} \ll r_o. \quad (\text{C } 3)$$

REFERENCES

- ANUFRIEV, A. P. 1994 The influence of solid core on Earth’s hydrodynamics. *Geophys. Astrophys. Fluid Dyn.* **77**, 15–25.
- AURNOU, J., BRITO, D. & OLSON, P. 1996 Mechanics of inner core super-rotation. *Geophys. Res. Lett.* **23**, 3401–3404.
- BENTON, E. R. & LOPER, D. E. 1969 On the spin-up of an electrically conducting fluid Part 1. The unsteady hydrodynamic Ekman–Hartmann boundary-layer problem. *J. Fluid Mech.* **39**, 561–586.
- BRAGINSKY, S. I. 1992 The Z model of the geodynamo with an inner core and the oscillations of the geomagnetic dipole. *Geomag. Aeron.* **29**, 98–103.
- DORMY, E., CARDIN, P. & JAULT, D. 1997 MHD flow in a slightly differentially rotating spherical shell, with conducting inner core, in a dipolar magnetic field. *Earth Planet. Sci. Lett.* submitted.
- ELTAYEB, I. A. & ROBERTS, P. H. 1970 On the hydromagnetics of rotating fluids. *Astrophys. J.* **162**, 699–701.
- GILMAN, P. A. & BENTON, E. R. 1968 Influence of an axial magnetic field on the steady linear Ekman boundary layer. *Phys. Fluids* **11**, 2397–2401.
- GLATZMAIER, G. A. & ROBERTS, P. H. 1995a A three-dimensional convective dynamo solution with rotating and finitely conducting inner core and mantle. *Phys. Earth Planet. Inter.* **91**, 63–75.
- GLATZMAIER, G. A. & ROBERTS, P. H. 1995b A three-dimensional self-consistent computer simulation of a geomagnetic reversal. *Nature* **377**, 203–209.
- GLATZMAIER, G. A. & ROBERTS, P. H. 1996a An anelastic evolutionary geodynamo simulation driven by compositional and thermal convection. *Physica D* **97**, 81–94.
- GLATZMAIER, G. A. & ROBERTS, P. H. 1996b The rotation and magnetism of Earth’s inner core. *Science* **274**, 1887–1891.
- GREENSPAN, H. P. 1968 *The Theory of Rotating Fluids*. Cambridge University Press.
- GUBBINS, D. 1981 Rotation of the inner core. *J. Geophys. Res.* **86**, 11695–11699.
- HIDE, R. 1995a The topographic torque on a bounding surface of a rotating gravitating fluid and the excitation by core motions of decadal fluctuations in the Earth’s rotation. *Geophys. Res. Lett.* **22**, 961–964.

- HIDE, R. 1995*b* Reply. *Geophys. Res. Lett.* **24**, 3563–3565.
- HOLLERBACH, R. 1994 Magnetohydrodynamic Ekman and Stewartson layers in a rotating spherical shell. *Proc R. Soc. Lond. A* **444**, 333–346.
- HOLLERBACH, R. 1996 Magnetohydrodynamic shear layers in a rapidly rotating plane layer. *Geophys. Astrophys. Fluid Dyn.* **82**, 281–280.
- HOLLERBACH, R. & JONES, C. A. 1993*a* A geodynamo model incorporating a finitely conducting inner core. *Phys. Earth Planet. Inter.* **75**, 317–327.
- HOLLERBACH, R. & JONES, C. A. 1993*b* Influence of the Earth's inner core on geomagnetic fluctuations and reversals. *Nature* **365**, 541–543.
- HOLLERBACH, R. & JONES, C. A. 1995 On the magnetically stabilising role of the Earth's inner core. *Phys. Earth Planet. Inter.* **87**, 171–181.
- JAULT, D. 1995 Model Z by computation and Taylor's condition. *Geophys. Astrophys. Fluid Dyn.* **79**, 99–124.
- JAULT, D. 1996 Sur l'inhibition de la régénération du champ magnétique dans certains modèles de dynamo planétaire en présence d'une graine solide. *C.R. Acad. Sci. Paris IIa* **323**, 451–458.
- JONES, C. A., LONGBOTTOM, A. W. & HOLLERBACH, R. 1995 A self-consistent convection driven dynamo model, using a mean field approximation. *Phys. Earth Planet. Inter.* **92**, 119–141.
- KLEERIN, N., ROGACHEVSKII, I. & RUZMAIKIN, A. A. 1993 Ekman–Hartmann boundary layers and length of the day variations. In *The Cosmic Dynamo* (ed. F. Krause, K.-H. Rädler & G. Rudiger), pp. 453–455. Kluwer, Dordrecht.
- LONGBOTTOM, A. W., JONES, C. A. & HOLLERBACH, R. 1995 Linear magnetoconvection in a rotating spherical shell, incorporating a finitely conducting inner core. *Geophys. Astrophys. Fluid Dyn.* **80**, 205–227.
- LOPER, D. E. 1970*a* General solution for the linearised Ekman–Hartmann layer on a spherical boundary. *Phys. Fluids* **13**, 2995–2998.
- LOPER, D. E. 1970*b* Steady hydromagnetic boundary layer near a rotating, electrically conducting plate. *Phys. Fluids* **13**, 2999–3002.
- LOPER, D. E. & BENTON, E. R. 1970 On the spin-up of an electrically conducting fluid Part 2. Hydromagnetic spin-up between infinite flat insulating plates. *J. Fluid Mech.* **43**, 785–799.
- MALKUS, W. V. R. & PROCTOR, M. R. E. 1975 The macrodynamics of α -effect dynamos in rotating fluids. *J. Fluid Mech.* **67**, 417–443.
- NIKITINA, L. V. & RUZMAIKIN, A. A. 1990 A flow inside the Earth created by a relative rotation of the mantle and internal solid core. *Geomag. Aeron.* **30**, 127–131.
- OLSON, P. & GLATZMAIER, G. A. 1995 Magnetoconvection in a rotating spherical shell: structure of flow in the outer core. *Phys. Earth Planet. Inter.* **92**, 109–118.
- PHILANDER, S. G. H. 1971 On the flow properties of a fluid between concentric spheres. *J. Fluid Mech.* **47**, 799–809.
- PROUDMAN, I. 1956 The almost rigid rotation of a viscous fluid between concentric spheres. *J. Fluid Mech.* **1**, 505–516.
- ROBERTS, P. H. 1988 Future of geodynamo theory. *Geophys. Astrophys. Fluid Dyn.* **44**, 3–31.
- RUZMAIKIN, A. 1989 A large-scale flow in the Earth core. *Geomag. Aeron.* **29**, 299–303.
- RUZMAIKIN, A. 1993 On the role of rotation of the internal core relative to the mantle. In *Theory of Solar and Planetary Dynamos* (ed. M. R. E. Proctor, P. C. Mathews & A. M. Rucklidge), pp. 265–270. Cambridge University Press.
- SARSON, G. R., JONES, C. A. & LONGBOTTOM, A. W. 1997 Convection driven geodynamo models of varying Ekman number. *Geophys. Astrophys. Fluid Dyn.* Submitted.
- SONG, X. & RICHARDS, P. G. 1996 Seismological evidence for differential rotation of the Earth's inner core. *Nature* **382**, 221–244.
- STARSHENKO, S. V. 1993 Magnetohydrodynamic flows formed on the Earth's outer core boundaries. *J. Geomag. Geoelectr.* **45**, 1563–1574.
- STEENBECK, M. & HELMIS, G. 1975 Rotation of the Earth's solid core as a possible cause of declination, drift and reversals of the Earth's magnetic field. *Geophys. J. R. Astron. Soc.* **41**, 237–244.
- STEWARTSON, K. 1957 On almost rigid rotations. *J. Fluid Mech.* **3**, 299–303.
- STEWARTSON, K. 1966 On almost rigid rotations. Part 2. *J. Fluid Mech.* **26**, 131–144.
- SU, W. A., DZIEWONSKI, A. & JEANLOZ, R. 1996 Planet within a planet: Rotation of the inner core of Earth. *Science* **274**, 1883–1887.

244 *N. Kleeorin, I. Rogachevskii, A. Ruzmaikin, A. M. Soward and S. Starchenko*

TAYLOR, J. B. 1963 The magneto-hydrodynamics of a rotating fluid and the Earth's dynamo problem. *Proc R. Soc. Lond. A* **274**, 274–283.

VEMPATY, S. & LOPER, D. E. 1975 Hydromagnetic boundary layers in a rotating cylindrical container. *Phys. Fluids* **18**, 1678–1686.

VEMPATY, S. & LOPER, D. E. 1978 Hydrodynamic free shear layers in rotating flows. *Z. Angew. Math. Phys.* **29**, 450–461.

WHALER, K. & HOLME, R. 1996 Catching the inner core in a spin. *Nature* **382**, 205–206.